Selective extracellular stimulation of individual neurons in ganglia

2008 J. Neural Eng. 5 287

(http://iopscience.iop.org/1741-2552/5/3/003)

J. Neural Eng. **5** (2008) 287–309 doi:10.1088/1741-2560/5/3/003

Selective extracellular stimulation of individual neurons in ganglia

Hui Lu[1], **Cynthia A Chestek**[2,5], **Kendrick M Shaw**[1] **and Hillel J Chiel**[1,3,4]

[1] Department of Biology, Case Western Reserve University, Cleveland, OH 44106, USA
[2] Department of Electrical Engineering, Case Western Reserve University, Cleveland, OH 44106, USA
[3] Department of Biomedical Engineering, Case Western Reserve University, Cleveland, OH 44106, USA
[4] Department of Neurosciences, Case Western Reserve University, Cleveland, OH 44106, USA

E-mail: hxl75@case.edu, cindyc@stanford.edu, kms15@case.edu and hjc@case.edu

Received 14 April 2008
Accepted for publication 26 June 2008
Published 19 August 2008
Online at stacks.iop.org/JNE/5/287

Abstract
Selective control of individual neurons could clarify neural functions and aid disease treatments. To target specific neurons, it may be useful to focus on ganglionic neuron clusters, which are found in the peripheral nervous system in vertebrates. Because neuron cell bodies are found primarily near the surface of invertebrate ganglia, and often found near the surface of vertebrate ganglia, we developed a technique for controlling individual neurons extracellularly using the buccal ganglia of the marine mollusc *Aplysia californica* as a model system. We experimentally demonstrated that anodic currents can selectively activate an individual neuron and cathodic currents can selectively inhibit an individual neuron using this technique. To define spatial specificity, we studied the minimum currents required for stimulation, and to define temporal specificity, we controlled firing frequencies up to 45 Hz. To understand the mechanisms of spatial and temporal specificity, we created models using the NEURON software package. To broadly predict the spatial specificity of arbitrary neurons in any ganglion sharing similar geometry, we created a steady-state analytical model. A NEURON model based on cat spinal motor neurons showed responses to extracellular stimulation qualitatively similar to those of the Aplysia NEURON model, suggesting that this technique could be widely applicable to vertebrate and human peripheral ganglia having similar geometry.

(Some figures in this article are in colour only in the electronic version)

Introduction

Extracellular stimulation has been extensively used both clinically and experimentally. Clinically, extracellular stimulation has been used to activate neural tissues in prostheses in order to restore function, e.g. visual perception (Mokwa 2007, Winter *et al* 2007), auditory perception (Spelman 2006, Lenarz *et al* 2006), control of micturition (Gaunt and Prochazka 2006, Jezernik *et al* 2002) and spinal and motor cortical function (Barbeau *et al* 1999, Cioni *et al* 2007). It has also been used to block neural signals in order to treat movement disorders (Benabid *et al* 1996, Anderson and Lenz 2006) or suppress pain (De Ridder *et al* 2007). Experimentally, extracellular stimulation can be applied to demonstrate the causal role of a single neuron on an animal's behaviour. For example, Ferguson *et al* (1986, 1989) successfully induced egg laying in freely behaving *Aplysia* by selectively stimulating bag cells. More recently, extracellular microstimulation of small groups of neurons has been used to determine the causal relationships between neural circuitry, behaviour and cognition in higher vertebrates and humans (Cohen and Newsome 2004).

In many applications, efficient extracellular stimulation requires selective activation or inhibition of targeted populations, which we will refer to as *spatial specificity* in this paper. A variety of approaches has been used to

[5] Present address: Department of Electrical Engineering, Stanford University, Stanford, CA 94305, USA.

improve spatial specificity of stimulation. For example, microelectrodes have been proposed for selective stimulation in the central nervous system (McIntyre and Grill 2000, McCreery *et al* 2006). In the peripheral nervous system, several electrode devices have also been designed for selective nerve stimulation, including spiral electrodes (Naples *et al* 1988), helical electrodes (Tarver *et al* 1992), intrafascicular electrodes (McNaughton and Horch 1996) and flat interface nerve electrodes (Tyler and Durand 2002, Levanthal *et al* 2006). However, it still remains difficult to selectively stimulate individual neurons, particularly smaller ones that are buried deeply and surrounded by large neurons.

Previous work has analysed the mechanisms by which extracellular stimulation may excite or inhibit individual neurons. In particular, studies have shown that when the electrode is on the side of the soma opposite to the axon, anodic currents can be used to excite the neuron, whereas cathodic currents can be used to inhibit the neuron (Ranck 1975, Suihko 1998, Rattay 1999). To our knowledge, however, no studies have been done in which the target neuron has been recorded intracellularly.

To develop selective stimulation, it may be best to focus on neuron clusters (i.e. ganglia), which are found throughout the peripheral nervous system. In invertebrates, the cell bodies of the excitable neurons are found near the surface of the ganglion, whereas the axonal network is found within the neuropil (Horridge and Bullock 1965). Many neuron cell bodies are also found near the surface of vertebrate ganglia (e.g., dorsal root ganglia and sympathetic ganglia, Williams *et al* (1995)). McIntyre and Grill (2002) have demonstrated that a neuron can respond to extracellular stimulation in different ways depending on its position with respect to the electrode. Therefore, if one stimulates near the cell bodies in a ganglion, which we will refer to as extracellular ganglionic stimulation in this paper, it may be possible to selectively stimulate neurons that cannot be controlled by other extracellular stimulation methods. In addition, because the soma diameter of a neuron is usually larger than its axon diameter, the distance between the centres of two cell bodies is usually larger than that between two axons. This could provide better spatial specificity of stimulation.

Previous studies have demonstrated selective stimulation and recording of an individual neuron in freely behaving *Aplysia* (Parson *et al* 1983). Parson *et al*'s (1983) technique involved attaching fine wire electrodes to the protective sheath above the specific cell bodies and isolating them from the surrounding fluid with glue, which is technically challenging and does not provide a particularly good seal. Therefore, they were forced to use several milliamperes of stimulation current. While the technique improved spatial specificity, the high levels of stimulation current sometimes induced noxious responses in the animals. Warman and Chiel (1995) improved the technique for single cell recording *in vivo* by attaching a pipette electrode made of glass or plastic to the sheath of the ganglion, and gluing it in place to provide an isolated chamber for electrodes. In this paper, we will extend this technique to stimulation, demonstrating that it is possible to selectively activate or inhibit a single neuron by extracellular stimulation on the side of the soma opposite to the axon.

In addition, to understand the stimulation mechanisms and study their spatial and temporal specificity, we simulate *Aplysia* buccal neurons using the NEURON software package. We also create a steady-state analytical model to generalize the NEURON model's predictions of the spatial specificity to arbitrary neurons that have various sizes and geometric configurations.

Materials and methods

Experimental methods

Aplysia californica weighing 200–450 g (Marinus Scientific, Garden Grove, CA) were maintained in an aerated aquarium containing artificial seawater (Instant Ocean; Aquarium Systems, Mentor, OH) kept at 18 ± 1 °C.

Extracellular stimulating electrodes were made from single-barrelled capillary glass (catalogue #6150; A-M Systems, Everett, WA), pulled on a Flaming–Brown micropipette puller (model P-80/PC; Sutter Instruments, Novato, CA). Electrodes were backfilled with *Aplysia* saline (460 mM NaCl, 10 mM KCl, 22 mM $MgCl_2$, 33 mM $MgSO_4$, 10 mM $CaCl_2$, 10 mM glucose, 10 mM MOPS, pH 7.4–7.5), and placed in the saline above the surface of the ganglion. Their inner diameters were about 40 μm and their resistances were about 0.1 MΩ. Currents were supplied by a stimulus isolator (model A-360, WPI).

Intracellular recording electrodes were also made from single-barrelled capillary glass (catalogue #6150; A-M Systems, Everett, WA) pulled on a Flaming–Brown micropipette puller (model P-80/PC; Sutter Instruments, Novato, CA). Electrodes were backfilled with 3 M potassium acetate, and their resistances were 3–6 MΩ. The bridge was balanced for both stimulation and recording. Intracellular signals were amplified using a dc-coupled amplifier (model 1600; A-M Systems).

Nerve recording electrodes were made from polyethylene tubing (catalogue #427421; Becton Dickinson, Sparks, MD; outer diameter 1.27 mm, inner diameter 0.86 mm). Electrodes were backfilled with *Aplysia* saline. Nerve recording signals were amplified using an ac-coupled differential amplifier (model 1700; A-M Systems) and filtered using a 300 Hz high-pass filter and a 1 kHz low-pass filter.

To study the responses of neurons to extracellular stimulation near the cell bodies, animals were anaesthetized and the buccal ganglia were dissected out. The buccal ganglia were pinned caudal side up in *Aplysia* saline. The nerve of interest was suctioned into the tapered end of the nerve recording electrode and recorded simultaneously as the extracellular stimulation was applied (figure 1, right side schematic). When intracellular recordings were also performed, ganglia were desheathed to expose the cell bodies of the neurons. The cell body of each neuron of interest was impaled by an intracellular electrode for recording, while it was simultaneously stimulated by an extracellular electrode (figure 1, left side schematic). During extracellular cathodic stimulation, we used the same intracellular recording electrode to induce multiple action potentials at a certain frequency by injecting a depolarizing current into the cell body.

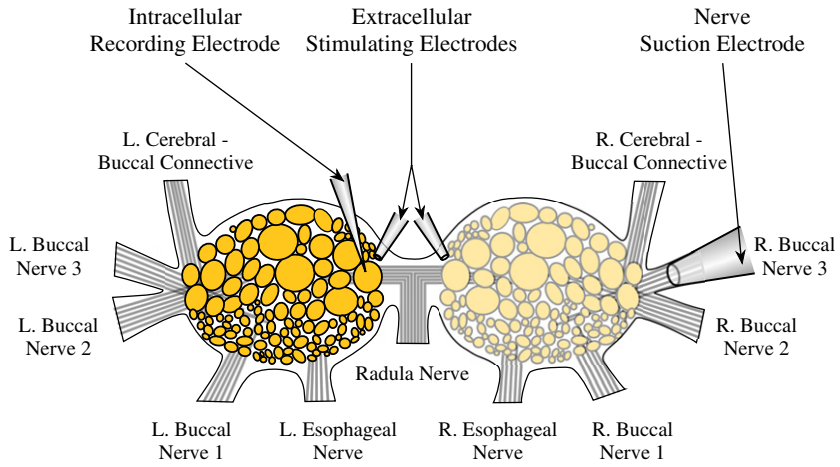

Figure 1. Schematic geometry of stimulating and recording electrodes in the *in vitro* experiments using *Aplysia* buccal ganglia. To illustrate intracellular recording and extracellular stimulation, the left semi-ganglion is shown with its protective sheath removed to expose the cell bodies. An extracellular stimulating electrode is placed directly above the soma of a neuron while an intracellular electrode is used to record from it simultaneously. To illustrate nerve recording and extracellular stimulation, the protective sheath is shown covering the right semi-ganglion. An extracellular stimulating electrode is placed above the sheath covering the soma of a neuron as a suction electrode is simultaneously used to record from the nerve containing its axon.

To measure the real membrane potential changes during extracellular stimulation, we subtracted the stimulation artefact from the intracellular recordings. The membrane potential is the difference between the internal and external voltages of the cell. Because the bath is grounded, the external voltage is normally zero, so the recording of the internal voltage of the cell can be used to represent the membrane potential. However, an extracellular current source will create an external voltage gradient, so in this case we cannot assume that the external voltage is zero. Thus, to obtain a more accurate value of the membrane potential during stimulation, we needed to estimate the external voltage as we recorded intracellularly. We first recorded the voltage in the bath near the soma with the intracellular electrode while applying extracellular stimulation at the current levels for every 100 μA in the range of 100–1000 μA. Then we penetrated the cell and measured the internal voltage during identical extracellular stimulation for every current level. Lastly, we subtracted the external voltage from the internal voltage that was recorded when applying the identical extracellular current, which we will refer to as the artefact-subtracted recording. Changes in the intracellular electrode resistance were negligible compared to the impedance of the amplifier and were therefore neglected.

In addition, to study the effects of the sheath on the neurons, we compared the minimum currents (i.e. threshold currents) needed to change the neural activity when the sheath was intact and after the sheath was removed. We placed the extracellular stimulating electrode above the sheath to stimulate the cell bodies underneath (figure 1, right schematic diagram). Because the sheath blocked the access of intracellular electrodes to the neurons, we instead recorded from the buccal nerve containing the axon of the targeted neuron. We first measured the threshold currents at different stimulating electrode locations when the sheath was intact. Afterwards, we removed the sheath partially or entirely and measured the threshold currents again at different stimulating electrode locations. Because we were not able to directly measure the electrode-to-soma distances with the sheath covering the neuron, we estimated them by adding the thickness of the sheath to the distances from the electrode to the sheath immediately covering the targeted neuron using the reticle of the microscope. We measured the thickness of the sheath that was removed as well as the thickness of the remaining sheath. We added these two values to estimate the original thickness of the sheath. The threshold currents before and after removing the sheath were nearly identical at the electrode locations in the range of 150–300 μm away from the neuron (for details, see Results section). Thus, the sheath of the buccal ganglion has a negligible effect on the threshold currents of neurons for extracellular ganglionic stimulation.

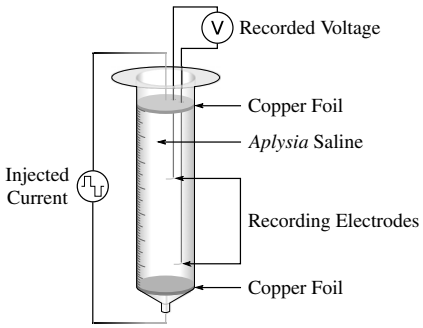

Figure 2. The experimental setup for measurements of the resistivity of *Aplysia* saline. Alternating positive and negative current pulses were applied to *Aplysia* saline in a conductance cell through two pieces of copper foil. The voltages across the two recording electrodes were measured as the separations between them were varied.

To estimate the resistivity of *Aplysia* saline, we performed a four-wire (Kelvin) resistance measurement (figure 2) (Light 1997). We applied 100 μA alternating positive and negative 3 ms current pulses at 200 Hz using two stimulus isolators

Table 1. Geometric parameters for Aplysia NEURON model.

Geometric parameter	Value
Soma	
Diameter	200 μm
Number of segments	101
Length of the 1st to the 100th segment	2 μm
Length of the 101th segment	0.002 μm
Axon	
Diameter	15 μm
Number of segments	200
Length of the 1st segment	51 μm
Length of the 2nd to the 200th segment	100 μm

(model A-360, WPI). We varied the separations of the two recording electrodes in a conductance cell and obtained the slope of the changing voltage versus separation. The resistivity of *Aplysia* saline was calculated by dividing the slope by the current amplitude and multiplying by the cross-sectional area of the conductance cell.

NEURON model simulations

To understand the mechanisms of extracellular ganglionic stimulation and study its spatial and temporal specificity, we developed models using the NEURON software package.

An unmyelinated neuron was simulated using the NEURON software package (Hines and Carnevale 1997), based on the simplified geometry of the *Aplysia* buccal neurons B4/B5. The parameters describing the geometry of this NEURON model are listed in table 1. *Aplysia* neurons do not have dendrites surrounding the cell bodies; rather, the dendrites emerge from the axons in the central neuropil (Kreiner *et al* 1987). Thus, we modelled the axon and dendrites as a single cylinder and modelled the soma as a sphere (figure 3(A)). The soma diameter was set to 200 μm based on a reticle measurement of B4/B5 using a microscope. The axon diameter was set to 15 μm based on the relative size of the soma and axon (Kreiner *et al* 1987). The axon length was set to about 20 mm based on a rough estimation of the nerve length. The soma sphere was divided into 100 segments of equal length (figure 3(A)). To increase the homogeneity of the electrical field across the soma as the electrode was moved through different angles, the soma segments were automatically rotated according to the stimulating electrode positions to remain perpendicular to the line between the electrode tip and the soma centre (figure 3(A), schematic diagrams 1 and 2). As a consequence, the connection location between the soma and the axon changed. When the 100th soma segment was connected to the axon, there was only one closed end at the 1st soma segment. However, when the 100th soma segment was not connected to the axon, there were two closed ends at both the 1st and the 100th soma segments. In order to eliminate this special case, we attached an additional very short soma segment (1/1000 the length of other soma segments) to the 100th segment as a small branch which would always act as the second closed end of the soma. When multiple electrodes were used to stimulate neurons (figure 14(C1)), the soma segments were rotated to point to the weighted average position of the electrodes. Then the axon was divided into 200 segments of equal length except the first axon segment whose length was the mean of one regular soma and axon segments. Increasing the number of segments by a factor of 10 while maintaining the overall neuronal geometry changed threshold currents by less than 0.1%.

The simulated neuron was represented by an equivalent electrical circuit (figure 3(B)). The midpoint of each segment was chosen to be a representation of the electrical node. The internal potential at the nth electrical node was represented by $V_i(n)$. The axial resistance of the nth electrical nodes was represented by $R_a(n)$, which was equal to

$$R_a(n) = \frac{4\rho_a}{\pi}\left(\frac{l(n)}{\mathrm{diam}(n)^2}\right), \qquad (1)$$

where $l(n)$ was the length of the nth segment, diam(n) was the diameter of the nth segment and ρ_a was the resistivity of the intracellular fluid of the neuron, which was estimated to be 200 Ω cm based on McIntyre and Grill (2002) and was in the range from 86 Ω cm to 410 Ω cm calculated from Hovey *et al* (1972). The electrical parameters of the NEURON model are listed in table 2. The dynamics of the fast sodium, slow potassium and leakage channels in the membrane were a modification of those originally described in the squid giant axon membrane by Hodgkin and Huxley (1952). We did not attempt to match the specific electrical parameters of the single-compartment model of B4/B5 (Ziv *et al* 1994), because we wished to generalize this NEURON model to many other excitable cells. The maximum conductances of fast Na^+ and slow K^+ channels, $\overline{g}_{Na}$ and $\overline{g}_K$, as well as the conductance of leakage channels, g_L, remained the same in the axon membrane as those in the Hodgkin–Huxley model. The reversal potential of the leakage channels was set to be −65 mV. To simulate the lower densities of Na^+ and K^+ channels in the soma compared to the axon, $\overline{g}_{Na}$ and $\overline{g}_K$ were reduced by a factor of 5 in the soma. The time constants of the Na^+ and K^+ channels were increased by linear scaling factors based on the ratios of the time constants of the Hodgkin–Huxley model to the time constants of *Aplysia* sensory neurons (Baxter *et al* 1999).

Extracellular stimulation was modelled by a point current source that was applied within an infinite homogeneous saline medium (McIntyre and Grill 1999), in which the X-axis was oriented along the axon and the Y-axis was perpendicular to the axon. The stimulating electrode was placed at (X_{elec}, Y_{elec}) relative to the centre of the soma at (0, 0). We assumed that the presence of the neuron did not affect the extracellular field created by this current source and that the extracellular potentials generated by the membrane currents of the neuron were negligible. We also assumed that the extracellular saline medium was homogeneous, with its resistivity estimated to be 19.3 Ω cm based on the measurements described above. In addition, we demonstrated that the sheath of the buccal ganglia had negligible effect on the threshold currents of neurons during extracellular stimulation (see previous Methods section and Results section below). Therefore, we used the same NEURON model to simulate neurons with or without the protective sheath.

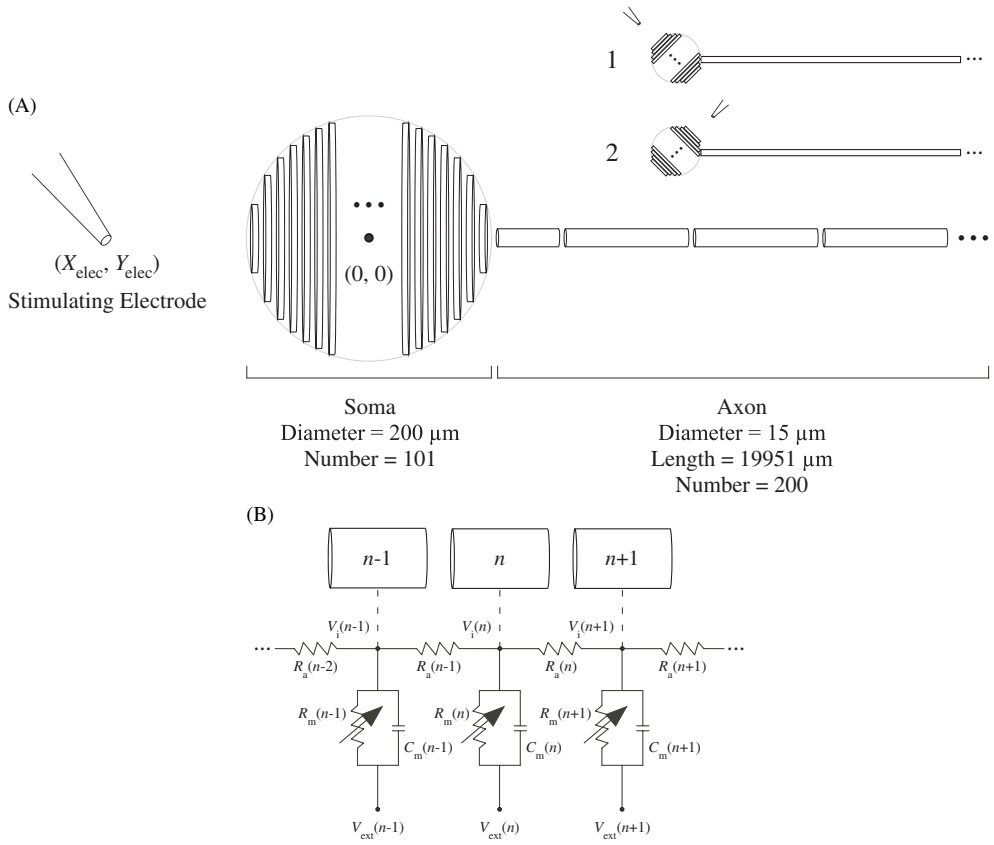

Figure 3. Morphology and equivalent electrical circuit of the Aplysia NEURON model. (A) Model morphology. The soma sphere is 200 μm in diameter and divided into 100 segments. An additional short soma segment is attached to the 100th soma segment as a small branch. The axon cylinder is 15 μm in diameter and 19 951 μm in length, and divided into 200 segments of equal length except the initial axon segment, whose length is 51 μm (mean of the regular soma and axon segment lengths). The centre of the soma is set to be (0, 0). The neuron is stimulated by an extracellular point source electrode at (X_{elec}, Y_{elec}), outside the neuron. The soma segments will be automatically rotated to be perpendicular to the line drawn from the stimulating electrode to the centre of the soma. See schematic diagrams 1 and 2. (B) Model equivalent electrical circuit. The midpoint of each segment is a representation of the electrical node. $V_i(n)$ represents the internal potential at the nth electrical node. $V_{ext}(n)$ represents the external voltage at the nth electrical node. $R_a(n)$ is the axial resistance between the nth and $(n+1)$th electrical nodes. Each compartment contains an active membrane resistance R_m and a membrane capacitance C_m.

Stimulation was modelled with an approach similar to Rattay (1989). The external voltage $V_{ext}(n)$ at any electrical node of the simulated neuron was determined by equation (2) (Rattay 1989):

$$V_{ext} = \frac{I}{4\pi\sigma_e r}, \tag{2}$$

where I is the magnitude of the applied extracellular current, σ_e is the conductivity of the extracellular medium ($\sigma_e = 1/\rho_e$) and r is the distance from the point current source to the nth node ($r = ((X_{elec} - X(n))^2 + (Y_{elec} - Y(n))^2)^{1/2}$). The ground electrode was assumed to be an infinite distance away. Therefore, these external voltages $V_{ext}(n)$ could be converted to the equivalent intracellular injected currents $I_{int}(n)$ at each node according to equation (3) (McIntyre and Grill 1999):

$$I_{int}(n) = 2\left(\frac{V_{ext}(n-1) - V_{ext}(n)}{R_a(n-1) + R_a(n)} - \frac{V_{ext}(n) - V_{ext}(n+1)}{R_a(n) + R_a(n+1)}\right). \tag{3}$$

These currents were applied to the neuron in monophasic pulses using the NEURON software package to view cellular voltages, including action potentials, over time. During extracellular cathodic stimulation, we injected additional depolarizing monophasic intracellular current pulses into the soma to induce multiple action potentials.

To investigate the spatial specificity when stimulating multiple cells, we added two more identical neurons to create a multiple-cell NEURON model. The centre of the middle neuron was set at (0, 0), and the centres of the neighbouring neurons were set at positions (0, −200) and (0, 200), respectively, with their axons parallel and pointing in the same direction. This simulated the geometry of the ganglion in which cell bodies are clustered together near the surface. The X-axis was along the axons and the Y-axis was perpendicular to the axons. The stimulating electrode was again placed at (X_{elec}, Y_{elec}) relative to the centre of the middle neuron at (0, 0). During cathodic inhibition, we injected depolarizing currents intracellularly into the cell bodies of all three neurons to induce a train of action potentials in each neuron.

To test the applicability of the technique to vertebrate neurons, we reconstructed a previously published model of cat spinal motor neurons (McIntyre and Grill 2000). Parameters

Table 2. Electrical parameters for Aplysia NEURON model.

Electrical parameter	Value
Extracellular resistivity of *Aplysia* saline (ρ_e)	19.3 Ω cm
Intracellular resistivity (ρ_a)	200 Ω cm
Membrane capacitance (C_m)	1 μF cm^{-2}
Fast Na$^+$ channels	
Max. conductance ($\overline{g}_{Na}$) in the soma	0.024 S cm^{-2}
Max. conductance ($\overline{g}_{Na}$) in the axon	0.12 S cm^{-2}
Activation term (α_m) of m gates	$-(0.15v + 6)(\exp(-0.1v - 4)) - 1)^{-1}$ [a]
Inactivation term (β_m) of m gates	$6\exp(-0.056v - 3.61)$[a]
Time constant of (τ_m) m gates	$((\alpha_m + \beta_m) * 3\hat{}(\text{celsius}/10 - 0.63))^{-1}$ [b]
Activation term (α_h) of h gates	$0.185\exp(-0.05v - 3.25)$ [a]
Inactivation term (β_h) of h gates	$2.65(\exp(-0.1v - 3.5) + 1)^{-1}$ [a]
Time constant of (τ_h) m gates	$((\alpha_h + \beta_h) * 3\hat{}(\text{celsius}/10 - 0.63))^{-1}$ [b]
Reversal potential (E_{Na})	50 mV
Slow K$^+$ channels	
Max. conductance ($\overline{g}_K$) in the soma	0.0072 S cm^{-2}
Max. conductance ($\overline{g}_K$) in the axon	0.036 S cm^{-2}
Activation term (α_n)	$-(0.008v + 0.442)(\exp(-0.1v - 5.5) - 1)^{-1}$ [a]
Inactivation term (β_n)	$0.1\exp(-0.0125v - 0.8125)$[a]
Time constant of (τ_n) m gates	$((\alpha_n + \beta_n) * 3\hat{}(\text{celsius}/10 - 0.63))^{-1}$ [b]
Reversal potential (E_K)	−77 mV
Leakage channels	
Conductance (g_L)	0.000 28 S cm^{-2}
Reversal potential (E_L)	−65 mV

[a] v is the membrane potential of a neuronal segment.
[b] Celsius is the centigrade environmental temperature.

Table 3. Geometric parameters for NEURON model of a cat spinal motor neuron.

Geometric parameter	Value
Soma	
Diameter	41.2 μm[a]
Number of segments	100
Length of each segment	0.412 μm
Axon (*node*)	
Diameter	9.6 μm[a]
Number of segments	200
Length of each segment	1.5 μm
Axon (*internode*)	
Diameter	12 μm[a]
Number of segments	200
Length of each segment	98.5 μm
Dendrite tree (*dendrite root*)	
Diameter	8 μm[a]
Total length	133 μm[a]
Number of segments	25
Length of each segment	5.32 μm
Dendrite tree (*dendrite branch*)	
Diameter	5.04 μm[a]
Total length	133 μm[a]
Number of segments	25
Length of each segment	5.32 μm

[a] McIntyre and Grill (2000).

of the model are presented in table 3. Qualitatively, results are similar to those obtained for the generic model of invertebrate neurons presented here. Results for this model are shown at the end of the paper (figure 18).

Analytical model

To generalize predictions about spatial specificity to arbitrary neurons that have various sizes and geometric configurations, and to provide a way to readily predict the magnitude of the threshold currents needed to stimulate a neuron, we created a steady-state analytical model. We represented the neuron as a semi-infinite axon in this model. The tip of the new axon was placed at the centre of the original soma, based on the work of Lee and Grill (2005) showing that the cytoplasmic potential in an isolated cell stimulated by a point source will approach the potential at its equator. The new axon was capped with a resistor equivalent to the total membrane resistance of the original soma.

We then examined the influence of an extracellular electric field on this new axon. A point current source was placed at a negative position along the X-axis. We assumed that the effects of the neuron on the extracellular electric field were negligible, and used a steady-state form of the cable equation to model the membrane potential in the axon (see appendix A for detailed derivation). We will refer to this model as the full analytical model.

While the resulting equation needed to be evaluated numerically, we found that we were able to approximate it with less than 6% error using the following equation when the current source was placed over the range of one to three length constants (or one-fifth to three length constants if γ, the normalized soma resistance, was greater than 1) away from the tip of the new axon:

$$\kappa_{th} = \left(\frac{20\alpha^2}{3} + \frac{(7\alpha^2 + 32\alpha + 2)\alpha\gamma}{4\sqrt{\alpha} + 2\alpha\gamma}\right)(1 + \nu_{th})\sec(\theta), \quad (4)$$

where κ_{th} is the normalized threshold current (the threshold current divided by $-4\pi\sigma_e E_m$, where σ_e is the conductivity of the extracellular medium and E_m is the resting membrane potential), α is the normalized distance from the centre of the soma to the extracellular stimulating electrode ($\alpha = d/\lambda$, where λ is the length constant of the axon and d is the distance from the centre of the soma to the point current source), γ is the normalized soma resistance ($\gamma = r_s/(r_i\lambda)$, where r_s is the total resistance across the membrane of the soma and r_i is the internal resistance per unit length in the axon), v_{th} is the normalized threshold potential ($v_{th} = -V_{th}/E_m$, where V_{th} is the threshold potential) and θ is the angle between the axon and the line drawn from the current source to the axon (see appendix A). We will refer to equation (4) as the simplified analytical model.

We performed two sets of simulations to determine the constants for the simplified analytical model when comparing it with the NEURON model. First, we determined the length constant λ by injecting a small intracellular current into the NEURON model axon and measuring the rate of membrane potential decrease with distance. For example, the length constant was about 514 μm for the simulated neuron with the soma diameter of 200 μm and the axon diameter of 15 μm, and the length constant was 351 μm for the neuron with half the soma and axon diameters. Second, we estimated v_{th} by measuring the threshold currents when extracellularly stimulating the NEURON model axon along the axonal axis at distances of 100–300 μm and fitting the results to the simplified analytical model.

Results

In this paper, we will describe and analyse a technique that is able to selectively activate and inhibit individual neurons by extracellular stimulation near the cell bodies in ganglia. For this purpose, we seek to (1) understand how extracellular ganglionic stimulation activates and inhibits neurons, (2) explore an important factor for selective stimulation, i.e. threshold current, (3) experimentally demonstrate whether it is possible to selectively activate and inhibit an individual neuron using this technique, (4) study the characteristics of stimulation specificity, i.e. spatial and temporal specificity and (5) explore whether this technique could be applicable to vertebrate peripheral ganglia that have neuron cell bodies clustering near the surface of the ganglia.

Mechanisms of extracellular ganglionic stimulation

Previous work demonstrated that a neuron can respond to extracellular stimulation in different ways and in different regions depending on its position relative to the stimulating electrode (McIntyre and Grill 2002, Iles 2005, Tehovnik *et al* 2006). Anodic stimulation on the side of the soma opposite to the axon had a lower threshold for exciting the cell than cathodic current (Ranck 1975, Rattay 1999), which is the opposite of what is seen in periaxonal stimulation. Similarly, cathodic stimulation from this side could induce inhibition of the cell. To examine quantitatively the voltage changes resulting from either anodic or cathodic extracellular stimulation, we constructed a NEURON model. We first examined how the same neuronal segment (e.g., the axon hillock) responds differently to extracellular stimulation depending on the electrode position. We measured the membrane potential changes of the axon hillock as we moved the stimulating electrode along the axonal axis from (−500, 200) to (2000, 200). The effects of extracellular electrical fields on axon membrane potentials have been well described (Rattay 1989). It is well known that anodic currents hyperpolarize the area immediately below the electrode while depolarizing the distal area. Therefore, when the electrode is placed near the axon hillock (figure 4(A), schematic 2), anodic currents strongly hyperpolarize the axon hillock so that the suppression will dominate. When the electrode is placed far away from the axon hillock (figure 4(A), schematic 3), anodic currents weakly depolarize the axon hillock which will not overcome the suppression due to strong hyperpolarization in the axonal areas immediately below the electrode. Furthermore, anodic currents applied on the side of the soma opposite to the axon (figure 4(A), schematic 1) weakly depolarize the axon hillock while strongly hyperpolarizing the soma. However, unlike the effects of distal axon stimulation (figure 4(A), schematic 3), this depolarization in the axon hillock will dominate because the axon hillock contains many more voltage-gated sodium channels than does the soma.

The effects of cathodic stimulation on a neuron are the reverse. Cathodic currents strongly depolarize the axon hillock when applied near it (figure 4(B), schematic 2). In contrast, cathodic currents weakly hyperpolarize the axon hillock as the electrode is placed far away from it (figure 4(B), schematics 1 and 3). While stimulating the distal axon, the weak hyperpolarization of the axon hillock cannot suppress the neuron's excitatory response to the distal axon depolarization. However, when stimulating on the side of the soma opposite to the axon, the hyperpolarization in the axon hillock can inhibit the neuron because of the high density of voltage-gated sodium channels in the axon hillock.

We then examined how various neuronal segments respond differently to extracellular ganglionic stimulation with the same current source. We measured the membrane potential changes along the neuron as we fixed the electrode position at (−150, 0). Anodic stimulation hyperpolarizes the proximal and middle parts of the soma, while depolarizing the distal soma and the proximal axon segments (figure 5(A)). Thus, a sufficiently large depolarization could initiate action potentials in the proximal axon segments, which then propagate throughout the rest of the neuron. This is consistent with the earlier modelling studies of Rattay (1999) who noted that spike initiation occurred in the proximal axon, but not at the hillock itself. Because of the low density of voltage-gated sodium channels, the hyperpolarization in the local soma segments will not be able to suppress the neuron's activity. The effects of cathodic currents on the neuronal segments are the reverse (figure 5(B)). Cathodic stimulation depolarizes the proximal and middle parts of the soma, while hyperpolarizing the distal soma and the proximal axon segments. Because

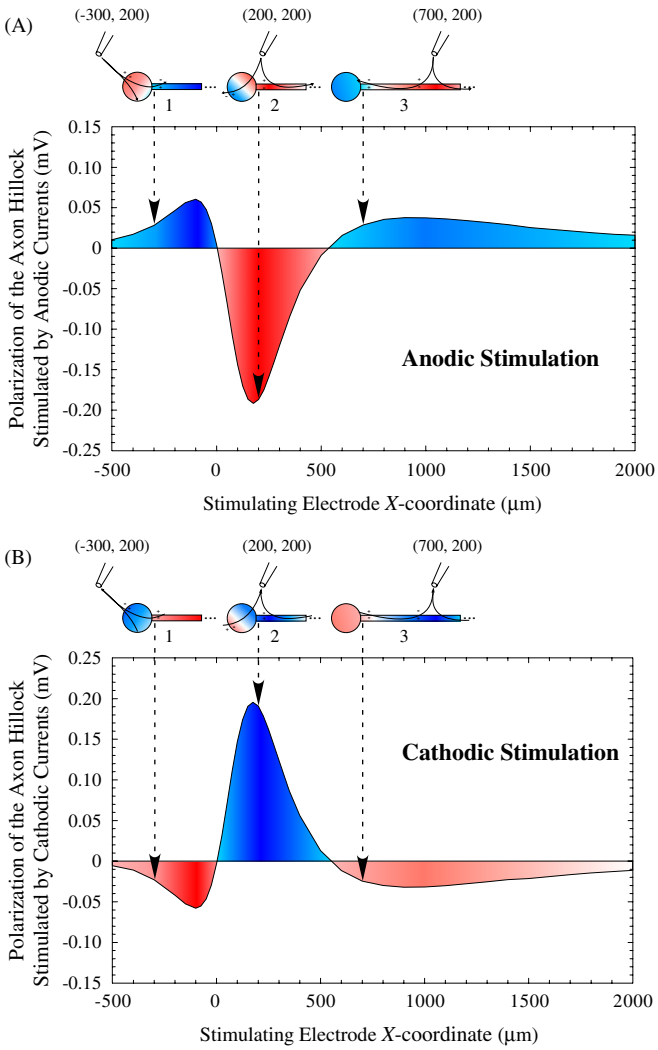

Figure 4. The polarization of the axon hillock varies as the extracellular stimulating electrode is placed at different positions. The membrane potential changes at the steady state were measured in the NEURON model. Positive membrane potential changes represent depolarization and negative membrane potential changes represent hyperpolarization. (A) A 100 ms current pulse of 10 μA was applied at a variety of locations (X_{elec}, 200), over the range from $X_{\text{elec}} = -500$ μm to $X_{\text{elec}} = 2000$ μm. Anodic currents depolarize the hillock as the stimulating electrode is placed on the side of the soma opposite to the axon, hyperpolarize the hillock as the electrode is placed near the hillock and depolarize the hillock again as the electrode is placed on the distal axon. (B) A 100 ms current of -10 μA was also applied at a variety of locations (X_{elec}, 200), over the range from $X_{\text{elec}} = -500$ μm to $X_{\text{elec}} = 2000$ μm. The effects of cathodic currents on the axon hillock are the reverse. The schematics show the stimulating electrode locations, current flows of positive and negative charges and the approximate membrane potential changes along the neuron. For each schematic, the large dashed arrow indicates the membrane potential change at the axon hillock for the electrode location shown in this schematic. The darker colour in both figures and schematics represents greater local depolarization.

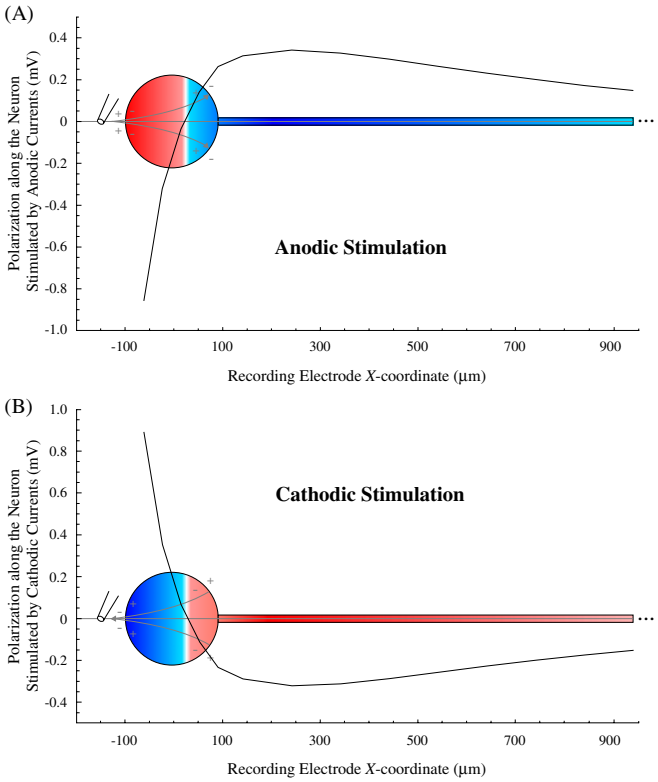

Figure 5. The polarization along the neuron by extracellular ganglionic stimulation. The membrane potential changes at the steady state were measured in the NEURON model. Positive membrane potential changes represent depolarization and negative membrane potential changes represent hyperpolarization. (A) A 100 ms current pulse of 10 μA was applied at $(-150, 0)$. Anodic currents hyperpolarize the proximal and middle soma while depolarizing the distal soma and proximal axon. (B) A 100 ms current of -10 μA was also applied at $(-150, 0)$. Cathodic currents depolarize the proximal and middle soma while hyperpolarizing the distal soma and proximal axon. Grey arrows indicate the current flows of positive and negative charges. Darker colour in the schematic neurons represents greater local depolarization.

the axon contains many more voltage-gated sodium channels than does the soma, the hyperpolarization in the proximal axon would dominate and thus inhibit the neuron. Therefore, we used anodic currents to activate neurons and cathodic currents to inhibit neurons during ganglionic stimulation on the side of the soma opposite to the axon.

Qualitative comparisons between experimental results and the NEURON model's predictions

To experimentally validate the effects of extracellular currents applied on the side of the soma opposite to the axon, we compared the neural responses obtained from *in vitro* electrophysiological experiments with those predicted by the NEURON model.

The NEURON model predicted that anodic currents would activate a neuron when applied on the side of the soma opposite to the axon. A 6 ms anodic current pulse was applied to the simulated neuron. Anodic stimulation strongly hyperpolarized the tip of the soma and weakly hyperpolarized the middle of the soma (figure 6(A); three black arrows point to the peaks of action potentials; the two top grey arrows indicate the hyperpolarization). However, the initial part of the axon was depolarized to generate an action potential, which

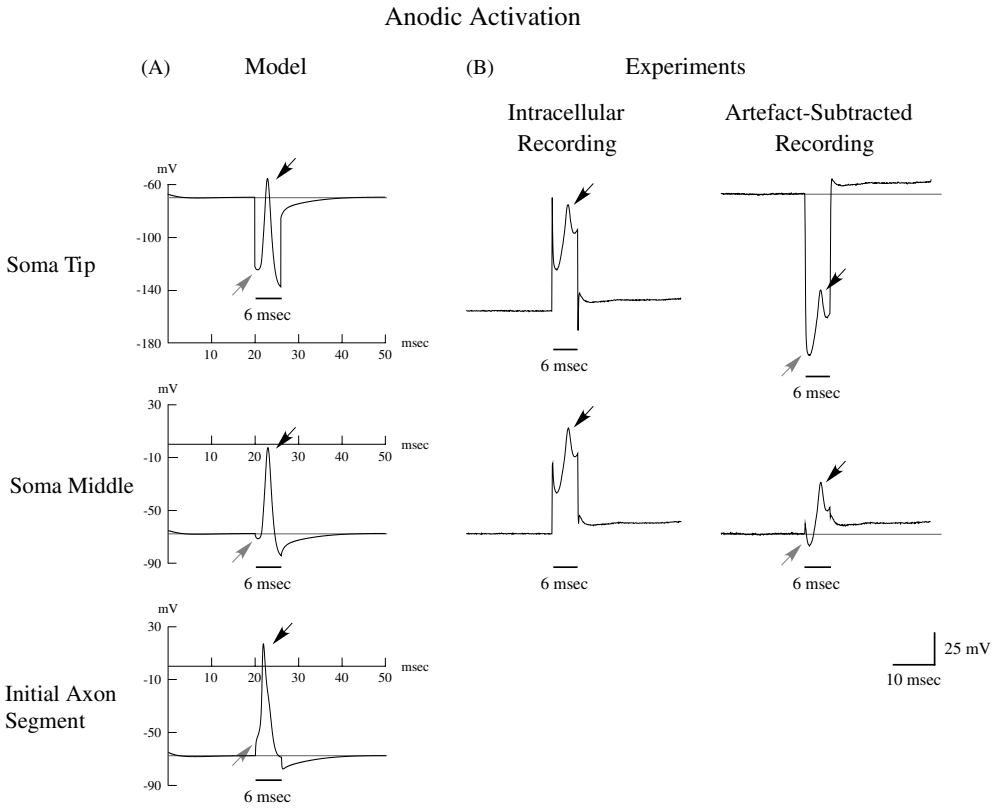

Figure 6. Qualitative comparisons between experimental results and the NEURON model's predictions: anodic currents activate a neuron by extracellular stimulation on the side of the soma opposite to the axon. (A) The neural responses due to anodic stimulation in the NEURON model. Anodic currents strongly hyperpolarized the tip of the soma and weakly hyperpolarized the middle of the soma, while depolarizing the initial axon segment to generate an action potential. (B) The intracellular recordings and artefact-subtracted recordings during anodic stimulation (for details, see Methods section). Both the intracellular recordings and artefact-subtracted recordings show an action potential at each site in the soma. The artefact-subtracted recordings also show strong hyperpolarization at the tip of the soma and slight hyperpolarization at the middle of the soma. The bars indicate the timing of extracellular stimulation. The grey lines show the resting membrane potentials. The grey arrows indicate the polarizations of the membrane. Each black arrow points to the peak of the action potential.

then propagated back to the soma (figure 6(A); the bottom grey arrow indicates the depolarization). Because of the high density of voltage-gated sodium channels in the initial axon segments, the hyperpolarization of the soma could not suppress the neuron's activation.

To demonstrate anodic activation experimentally, we intracellularly recorded from both the tip and the middle of a soma in a desheathed ganglion as we simultaneously applied a 6 ms anodic current pulse above the soma. The intracellular recordings showed that the neuron was excited to fire an action potential at both sites of the soma (figure 6(B); the two left black arrows point to the peaks of action potentials). However, the real polarization of the neuron at each soma site was embedded in the stimulation artefact. Thus, we subtracted the artefact from the intracellular recordings to show both the action potentials and the polarizations of the neuron (for details, see Methods section). We found that the tip of the soma was strongly hyperpolarized while the middle of the soma was only weakly hyperpolarized due to anodic stimulation (figure 6(B); the two grey arrows indicate the hyperpolarization; the two middle black arrows point to the peaks of action potentials). In addition, the action potentials occurred despite the hyperpolarization in both sites of the soma. Therefore, the experimental results qualitatively validate the NEURON model's prediction that anodic activation is likely to be due to depolarization of the initial axon segments.

The NEURON model also predicted that cathodic currents would inhibit a neuron when applied on the side of the soma opposite to the axon. A 300 ms intracellular current pulse was injected into both the tip and the middle of the simulated neuron to generate multiple action potentials. Then a 100 ms cathodic extracellular current pulse was also applied to the simulated neuron (figure 7(A)). Cathodic currents hyperpolarized the initial part of the axon, blocking action potentials, whereas they strongly depolarized the tip of the soma and weakly depolarized the middle of the soma (figure 7(A); note the grey lines, indicating the steady-state membrane potential in response to the intracellular current alone). Thus, cathodic currents inhibit the neuron by directly hyperpolarizing the initial axon segments.

To demonstrate cathodic inhibition experimentally, we again recorded intracellularly from both the tip and the middle of the soma. We applied a 3 s intracellular current pulse to both soma sites to induce action potentials, and then applied a 1 s cathodic current pulse immediately above the

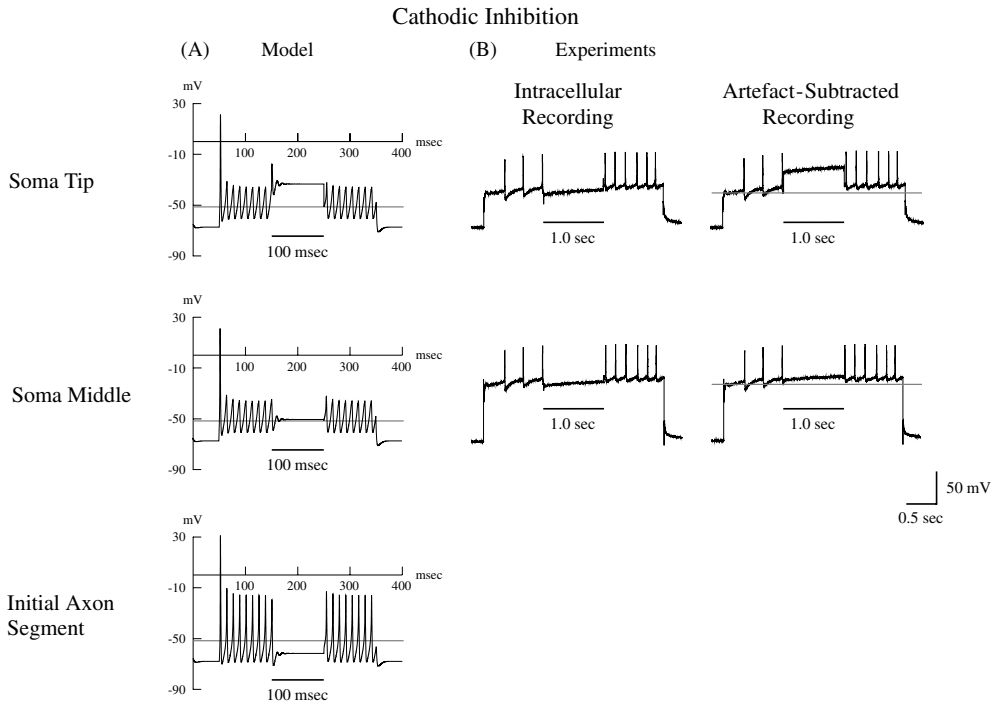

Figure 7. Qualitative comparisons between experimental results and the NEURON model's predictions: cathodic currents inhibit the neuron by extracellular stimulation near the cell bodies. (A) The neural responses due to cathodic stimulation in the NEURON model. Cathodic currents strongly depolarized the tip of the soma and weakly depolarized the middle of the soma, while hyperpolarizing the initial axon segment and blocking the action potentials. (B) The intracellular recordings and artefact-subtracted recordings during cathodic stimulation (for details, see Methods section). Both the intracellular recordings and artefact-subtracted recordings show that action potentials were completely blocked during extracellular stimulation at both sites in the soma. The artefact-subtracted recordings also show strong depolarization at the tip of the soma and slight depolarization at the middle of the soma. The bars indicate the timing of extracellular stimulation. The grey lines show the resting membrane potentials.

soma in a desheathed ganglion (figure 7(B)). The intracellular recordings showed that action potentials were completely blocked during cathodic extracellular stimulation at both sites in the soma. In the artefact-subtracted recordings, the tip of the soma was significantly depolarized during extracellular stimulation, whereas the middle of the soma was only slightly depolarized (figure 7(B); the grey lines correspond to the steady-state membrane potential in response to the intracellular current alone). Thus, the experimental results qualitatively validate the NEURON model's prediction that cathodic hyperpolarization of the initial axon segment will inhibit nerve cells.

Threshold currents

Stimulation specificity requires that a single neuron can be selectively activated or inhibited among a group of neurons (*spatial specificity*) or that single spikes can be selectively added to or removed from a firing pattern of an individual neuron (*temporal specificity*). To obtain stimulation specificity, we need to employ the minimum currents that are necessary for effective stimulation. Therefore, we defined the threshold current for anodic activation to be the minimum current required to activate an individual neuron to generate at least one action potential. The threshold current for cathodic inhibition was defined to be the minimum current needed to totally block all action potentials in an individual neuron driven by a fixed input (e.g., intracellular depolarizing current or synaptic input) during the inhibitory pulse.

To predict threshold currents at various electrode positions, we studied the relationship between threshold currents and the distances from the stimulating electrode to the soma via intracellular recordings (figure 1, left-side schematic). Consistent with previous studies (Stoney *et al* 1968, Nowak and Bullier 1996), the square root of threshold current for both anodic activation and cathodic inhibition increased as we moved the stimulating electrode away from the soma (figure 8; $n = 3$, $p < 0.05$). The NEURON model also suggested qualitatively similar linear relationships between the square root of the threshold current and the electrode-to-soma distance ($p < 0.05$ for the linear fits of the square root transformations of both the anodic and the cathodic model data). We noted that the threshold currents could be relatively low (e.g., 30–60 μA) when the electrode was placed very close to the cell bodies (e.g., at around 5 μm) based on the linear fits from the experimental data.

Do we need more current to stimulate neurons when the protective sheath of the ganglia is intact, which is very important if this technique is to be applied *in vivo*? To investigate this, we compared the threshold currents for anodic activation of a single neuron when the sheath was intact and after the sheath was removed. We applied anodic stimulation to the soma of the targeted neuron through the sheath and simultaneously recorded from the buccal nerve containing

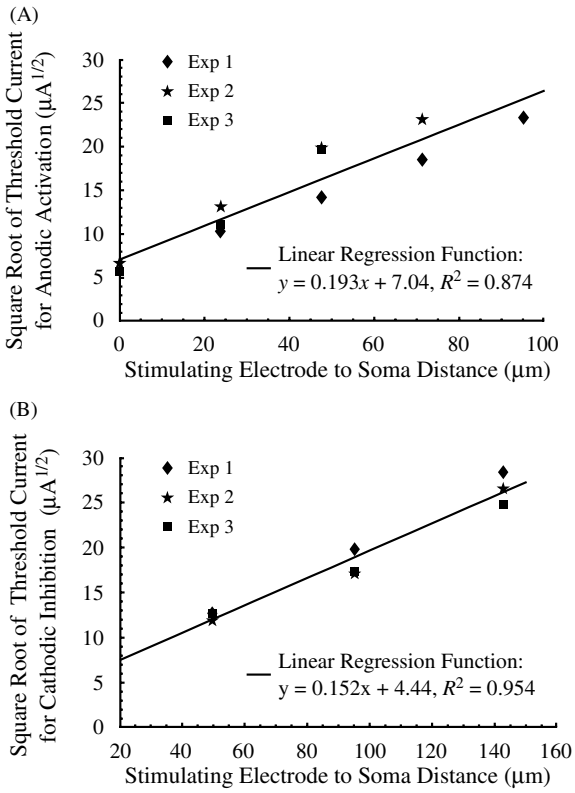

Figure 8. Threshold currents for both anodic activation and cathodic inhibition increase with the distance from the stimulating electrode to the soma. (A) The square root of the threshold current yields a linear fit over this range of the electrode-to-soma distance: $y = 0.193x + 7.04$ ($R^2 = 0.874$, $p < 0.05$). (B) The square root of the threshold current yields a linear fit over this range of the electrode-to-soma distance: $y = 0.152x + 4.44$ ($R^2 = 0.954$, $p < 0.05$).

its axon (figure 1, right-side schematic). We measured threshold currents at various stimulating electrode positions and estimated the electrode-to-soma distances (for details, see Methods section). The threshold currents of the same neuron were very close when the sheath was intact and after the sheath was removed (figure 9; $n = 3$). However, we noted that we did need more current to activate a neuron in an intact animal because the stimulating electrode cannot be placed very close to the neuron when the sheath is intact.

Selective activation and inhibition of an individual neuron

Can we selectively activate or inhibit an individual neuron by extracellular ganglionic stimulation? As shown in figures 8 and 9, the threshold currents of a neuron increase with the electrode-to-soma distance. As an electrode is moved along the surface of the ganglion, it will be closer to the cell bodies of some neurons and further from others. Thus, if we position the electrode over a certain range, extracellular currents should be able to selectively stimulate a single neuron.

To demonstrate selective activation, we intracellularly recorded simultaneously from the cell bodies of three adjacent neurons as we applied anodic extracellular currents above the soma of the targeted middle neuron in a desheathed ganglion (figure 10(A); $n = 8$). The intracellular recordings showed

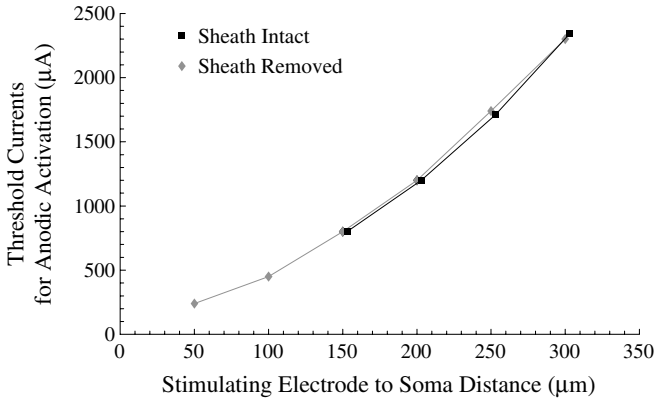

Figure 9. Threshold currents of the same neuron were very close when the sheath was intact and after the sheath was removed ($n = 3$; for details, see Methods section). This is one of the typical results of three replications (the sheath was entirely removed in this replication). Black square symbols indicate the threshold currents of the neuron when the sheath was intact. Grey diamond symbols indicate the threshold currents after removing the sheath of the same preparation.

that at the threshold current, the middle neuron fired an action potential following the stimulating artefact (figure 10(B); note the black arrow pointing to the action potential). However, this current was not enough to activate the other two neurons. When 386% of the threshold current was applied, both the left and the middle neurons were excited to generate at least one action potential during or following the stimulation (figure 10(C); note the black arrows pointing to the action potentials). Finally, as we increased the current to 471% of the threshold current of the middle neuron, all three neurons were excited and generated at least one action potential during or following the stimulation (figure 10(D); note the black arrows pointing to the action potentials). Therefore, an individual neuron can be selectively activated without activating its neighbours.

To demonstrate selective inhibition of an individual neuron, we again recorded intracellularly from the cell bodies of three adjacent neurons simultaneously. A depolarizing current was injected into each soma to induce a train of action potentials. A cathodic extracellular current was applied above the soma of the targeted middle neuron (figure 11(A); $n = 3$). At the threshold current, cathodic stimulation only eliminated the action potentials in the middle neuron (figure 11(B)). With 208% of the threshold current of the middle neuron, both the left and the middle neurons were inhibited during the stimulation (figure 11(C)). Finally, as we increased the current to 358% of the threshold current of the middle neuron, all three neurons were inhibited during the stimulation (figure 11(D)). Therefore, an individual neuron can be inhibited selectively without suppressing the neighbouring neurons.

Spatial specificity for multiple neurons

The ability to selectively stimulate a single neuron among multiple neurons is one of the most important aspects of our technique, which we refer to as spatial specificity. It requires that the minimum current necessary to stimulate a given neuron

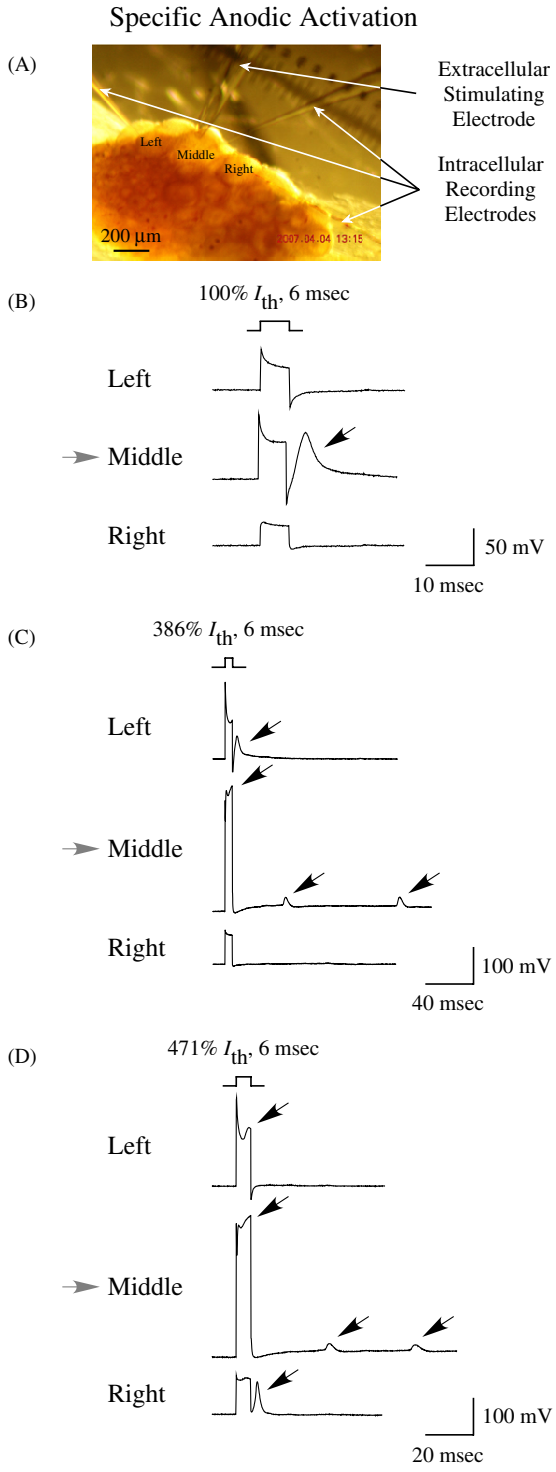

Figure 10. Anodic currents can selectively activate an individual neuron. (A) Experimental setup of the three intracellular recording electrodes and the extracellular stimulating electrode in a desheathed ganglion ($n = 8$; for details, see Methods section). (B) Only the middle targeted neuron was activated by the threshold current for anodic stimulation. (C) Both the left and middle neurons were activated by 386% of this threshold current. (D) All three neurons were activated by 471% of this threshold current. In (B)–(D), the grey arrows point to the targeted neuron, the duration of each pulse indicates the timing of stimuli and the black arrows point to the action potentials respectively. We sharpened the image of the lower right electrode in (A), which was present in the original picture but was slightly blurred.

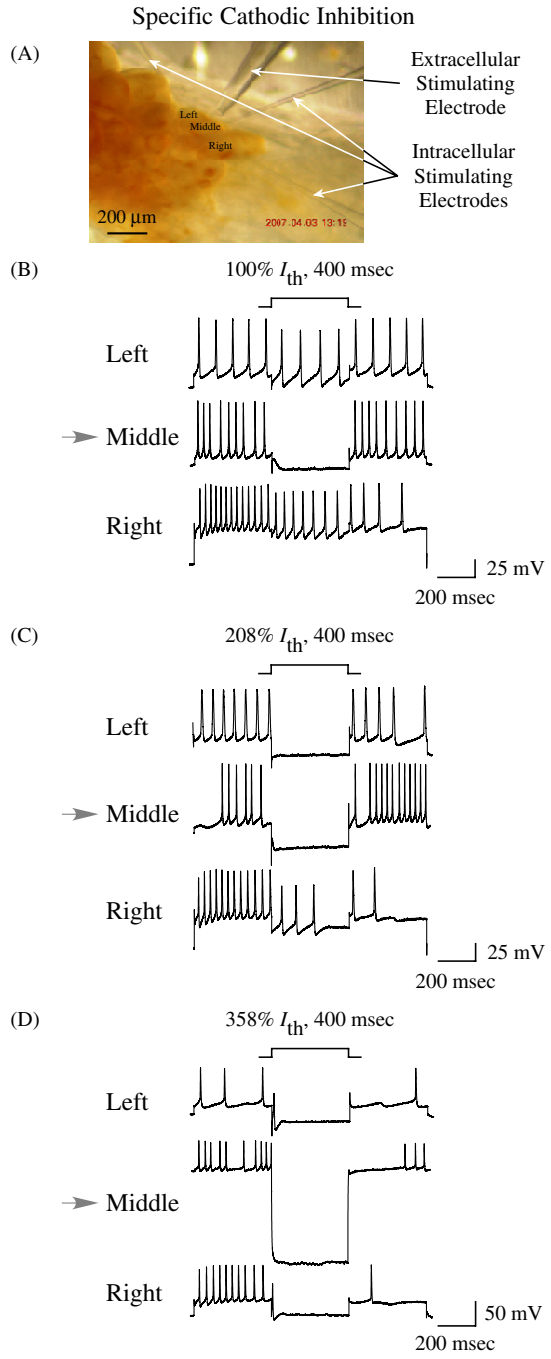

Figure 11. Cathodic currents can selectively inhibit an individual neuron. (A) Experimental setup of the three intracellular recording electrodes and the extracellular stimulating electrode in a desheathed ganglion ($n = 3$; for details, see Methods section). (B) Only the middle targeted neuron was inhibited by the threshold current for cathodic stimulation. (C) Both the left and middle neurons were inhibited by 208% of this threshold current. (D) All three neurons were inhibited by 358% of this threshold current. In (B)–(D), the grey arrows point to the targeted neuron.

is less than that needed to stimulate any other neuron by a reasonably large and reliable margin. In order to quantify the current window of spatial specificity, we defined it to be $(I_{\text{adjacent}} - I_{\text{neuron}})/I_{\text{adjacent}}$, where I_{adjacent} was the threshold current for an adjacent neuron and I_{neuron} was the threshold

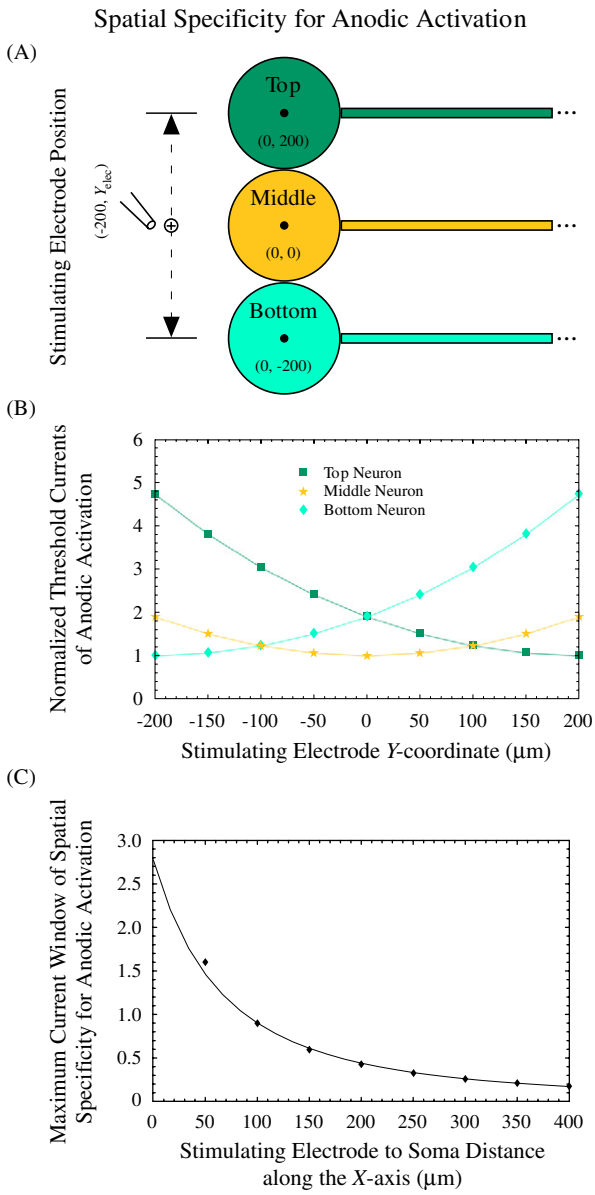

Figure 12. The spatial specificity for anodic activation predicted by the multiple-cell NEURON model. (A) Morphology of the NEURON model consisting of three identical adjacent neurons (for details, see Methods section). (B) The normalized threshold currents of the three neurons are predicted by the model as the stimulating electrode is moved along the line between (−200, −200) and (−200, 200). From $Y_{elec} = -99$ μm to $Y_{elec} = 99$ μm, the normalized anodic threshold currents of the middle neuron are lower than those of the other two neurons, so that the middle neuron can be selectively activated (note the star symbols and symmetric line). The maximum current window of spatial specificity occurs at $Y_{elec} = 0$ μm. (C) The maximum current window decreases as the stimulating electrode is moved away from the neurons along the X-axis.

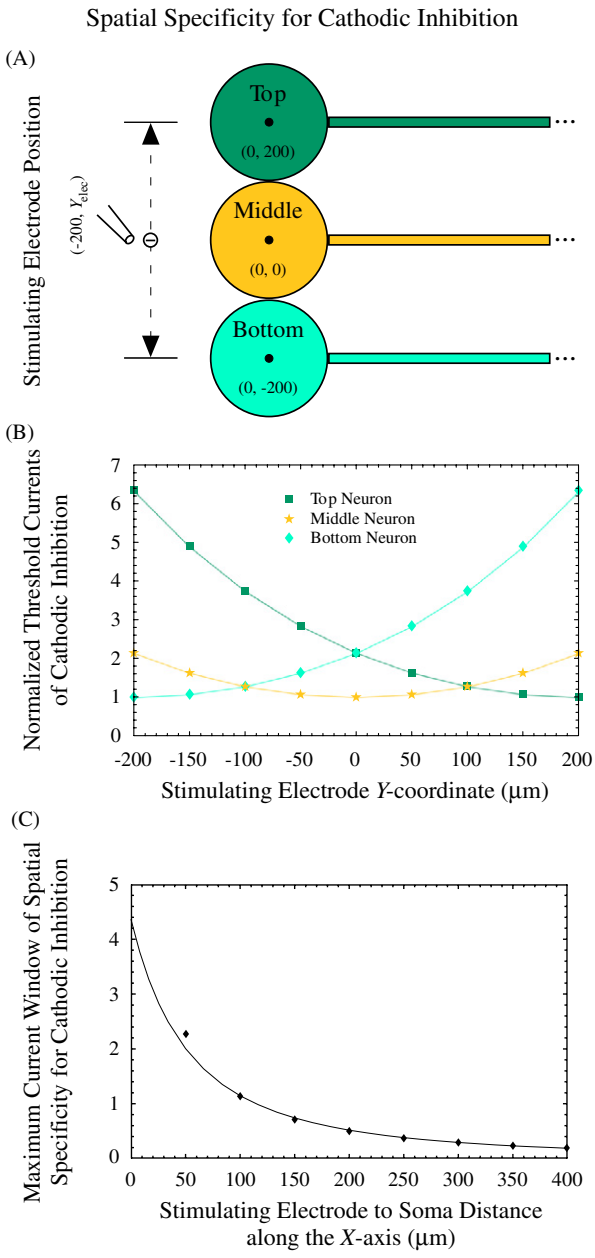

Figure 13. The spatial specificity for cathodic inhibition predicted by the multiple-cell NEURON model. (A) Morphology of the NEURON model consisting of three identical adjacent neurons (for details, see Methods section). (B) The normalized threshold currents of the three neurons are predicted by the model as the stimulating electrode is moved along the line between (−200, −200) and (−200, 200). From $Y_{elec} = -99$ μm to $Y_{elec} = 99$ μm, the normalized threshold currents of the middle neuron are lower than those of the other two neurons, so that the middle neuron can be selectively inhibited (note the star symbols and symmetric line). The maximum current window of spatial specificity occurs at $Y_{elec} = 0$ μm. (C) The maximum current window will decrease quickly as the stimulating electrode is moved away from the neurons along the X-axis.

current for the neuron of interest. In figures 10 and 11, we show large current windows of spatial specificity, which are 286% for anodic activation and 108% for cathodic inhibition.

To investigate the characteristics of spatial specificity, we created a multiple-cell NEURON model consisting of three adjacent neurons as described in the Methods section (figures 12(A) and 13(A)). We defined the X-axis to be along the axons and the Y-axis to be perpendicular to the axons. The X-coordinate of the stimulating electrode was fixed at 200 μm away from the centres of the cell bodies. The electrode was then moved along the Y-axis from the centre of the bottom neuron at $Y_{elec} = -200$ μm to the centre of the top neuron

at $Y_{elec} = 200$ μm. At each point, the threshold currents of all three neurons were recorded and normalized to be the percentage of the minimum threshold current of the targeted middle neuron. When the electrode was placed between $Y_{elec} = -99$ μm and $Y_{elec} = 99$ μm, the normalized threshold currents of the middle neuron were lower than those of the other two neurons for both anodic activation and cathodic inhibition (figures 12(B) and 13(B); note the star symbols and symmetric line). As a consequence, the middle neuron could be activated and inhibited selectively over this range. At $Y_{elec} = 0$ μm, we could obtain the maximum current windows of spatial specificity, which were 88.8% for anodic activation and 113.7% for cathodic inhibition. In addition, the sizes of these maximum current windows fell quickly (approximately as the inverse square of the electrode-to-soma distance) as the stimulating electrode was moved away (figures 12(C) and 13(C)).

How general are the spatial specificity results as the neuron geometry varies, in particular, as one neuron is further from the surface than the surrounding neurons? To address this question, we developed a steady-state analytical model (for details, see Methods section and appendix A) to predict the spatial specificity of arbitrary neurons that have various sizes and geometric configurations. We found that for the distances of interest (about one-third to three length constants from the soma), the simplified analytical model described in equation (4) provides an excellent approximation to the threshold current values from the NEURON model (figures 14(A2), (B2) and (C2); note the lines for the analytical model and the symbols for the NEURON model).

How does the spatial specificity change if the neurons of interest have different sizes? Since a small neuron has a higher threshold current than a large neuron, it might be difficult to stimulate a small neuron selectively if it is surrounded by large neurons. To explore this problem, we considered the case where a small neuron was surrounded by two large neurons. The parameters of the large neurons were the same as those used in the previous multiple-cell NEURON model containing three identical adjacent neurons (figure 12(A)). The soma and axon diameters of the small neuron were 100 μm and 7.5 μm, respectively, which were both half of those of the large neurons. We first examined the neural responses when all three neurons were aligned at the tips of their cell bodies with their axons parallel to each other (figure 14(A1)). We did the same measurements of threshold currents to determine spatial specificity. The targeted small middle neuron could be selectively activated. For example, the maximum current window was 11.2% when the stimulating electrode was 200 μm away along the *X*-axis from the tips of the cell bodies (figure 14(A2); note the arrow pointing down). Although it is smaller than the maximum current window shown above (figure 12), it is still sufficient for reliable selective stimulation. Similarly, the maximum current window was largest when the stimulating electrode was close to the neurons along the *X*-axis, and it fell as the electrode was moved away (data not shown).

How does specificity change if the neurons of interest have both different sizes and geometric configurations? One extreme case would occur if the targeted neuron was both smaller and further away from the surface. For example, the targeted small neuron and its neighbours could be aligned at their hillocks with their axons parallel to each other (figure 14(B1)). In fact, we observed that spatial specificity was now much worse: the targeted small neuron could not be selectively activated (figure 14(B2); note the arrow pointing up). In order to regain the spatial specificity of the targeted small neuron, we had to place the electrode immediately above it and between the two large adjacent neurons. For example, when the *X*-coordinate of the electrode was 50 μm from the tip of the small neuron, the maximum specificity window was about 75% of its minimum threshold current (data not shown). Previous work by Tarler and Mortimer (2004) studying axon stimulation showed that if one suppresses the activity in neighbouring axons, it was possible to regain spatial specificity. Based on this idea, we were able to restore the spatial specificity of the middle small neuron by adding two cathodic current sources directly above the two large adjacent neurons (figure 14(C)).

Temporal specificity for an individual neuron

In many applications, it is also crucial to control the firing frequency of a neuron by adding or removing specific spikes at precise times, which we refer to as temporal specificity. At the threshold current for anodic stimulation, one can use a low-frequency pulse train to generate a single action potential during or immediately following each single pulse. This makes it possible to control the firing frequency of the neuron by adding one action potential per pulse (figure 15). However, a higher current or pulse frequency may induce more than one action potential per pulse, making the neuron's firing frequency unpredictable. For example, we found that we could reliably drive B4/B5 to fire at frequencies up to 45 Hz using anodic pulse trains (data not shown), but not at higher frequencies. We were also able to add specific spikes to the firing pattern of B4/B5 (figure 15).

Similarly, at the threshold current for cathodic stimulation, we can also use a low-frequency pulse train to block a single action potential during a single pulse. This also allows the control of firing frequency by removing one action potential per pulse (figure 16). However, the pulse should be long enough to cover the duration of an action potential so that each pulse can eliminate one action potential. For example, we were able to control the spiking rates of B4/B5 when it was firing at frequencies lower than 45 Hz. We were also able to remove specific spikes during repetitive firing of B4/B5.

Generalization of the technique

To explore whether this technique can be generalized to neurons having varying morphologies in vertebrates, we examined the stimulation mechanisms under different conditions. First, we examined whether the size of the neuron would affect the mechanisms of extracellular ganglionic stimulation by comparing the membrane polarization along the neuron as we varied the soma and axon diameters. We found that in the simulated neuron with the original soma

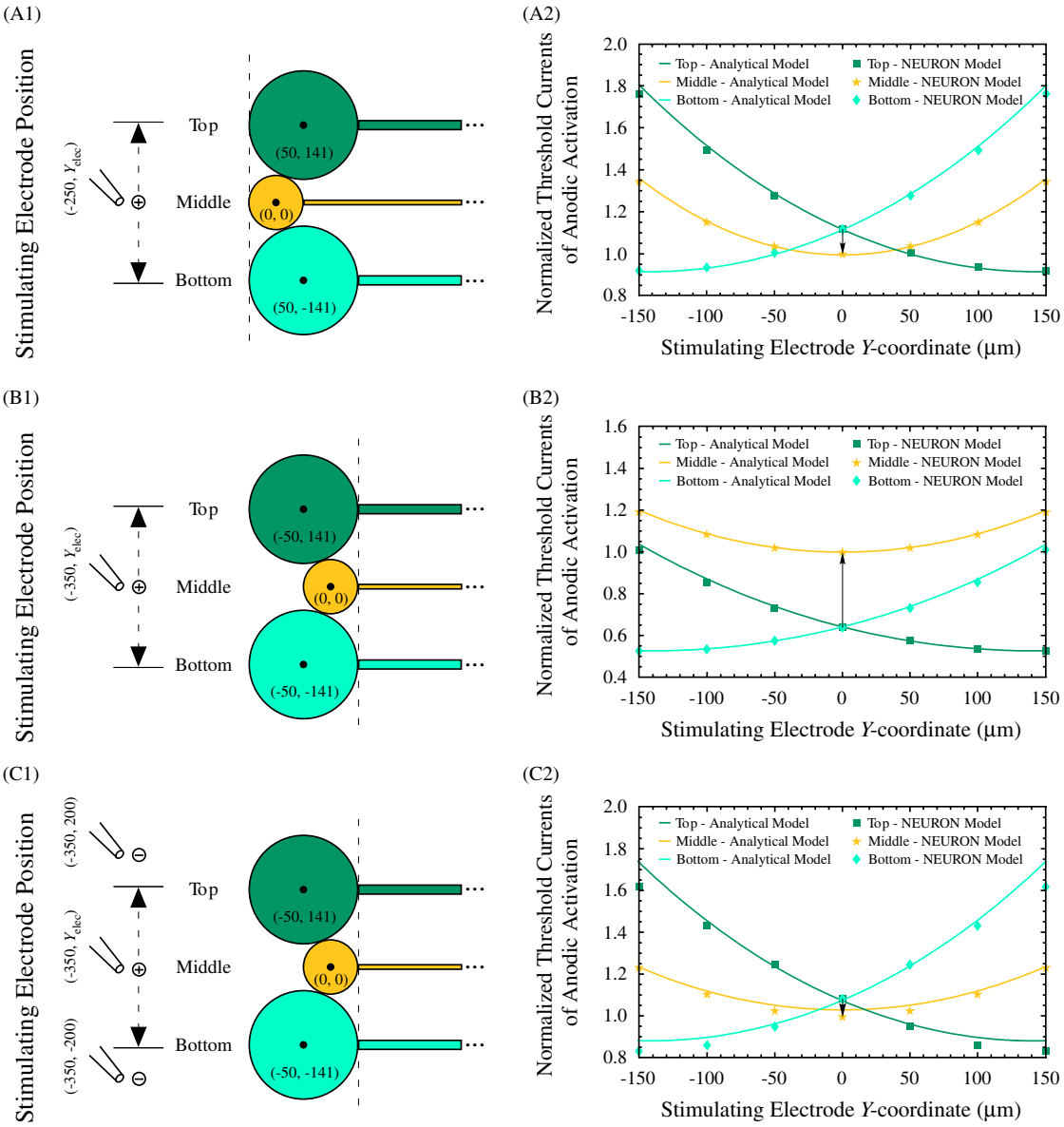

Figure 14. The spatial specificity for a group of neurons with different sizes and geometric configurations predicted by the NEURON model and the analytical model. (A1) Morphology of the NEURON model consisting of a small targeted neuron surrounded by two large neighbouring neurons, all aligned at their tips. (A2) The normalized threshold currents for anodic stimulation of these three neurons are predicted by both the NEURON model and the analytical model. The arrow pointing down indicates a positive specificity window (11.6%) for the targeted small neuron, so that it can be selectively stimulated. (B1) Morphology of the NEURON model when the targeted small neuron is buried more deeply; the three neurons are aligned at their hillocks. (B2) The normalized threshold currents for anodic stimulation of these three neurons are predicted by both the NEURON model and the analytical model. The arrow pointing up indicates a negative specificity window for the targeted small neuron, so that it cannot be selectively stimulated. (C1) Morphology of the NEURON model with the three neurons aligned at their hillocks and stimulated by three electrodes. Two additional stimulating electrodes are added to apply cathodic currents near the neighbouring large neurons. (C2) The normalized threshold currents for multiple-electrode stimulation of these three neurons are predicted by both the NEURON model and the analytical model. The arrow pointing down indicates a restored positive specificity window (8.3%) for the targeted small neuron, so that it can now be selectively stimulated.

diameter of 200 μm and axon diameters of 15 μm, the maximum membrane polarization occurred at the second axon segment, which would be the initiation site for generating or inhibiting action potentials (figure 17; black solid lines in both (A) and (B)). We fixed the axon diameter and then increased or reduced the soma diameter (figure 17(A); the grey solid line and black dashed line). Note that as we reduced the soma diameter to 41.2 μm, which was the value for a cat spinal motor neuron model developed by McIntyre and Grill (2000), the site of maximum membrane polarization shifted towards the end of the axon by a few axon segments (figure 17(A); the black dashed line). In contrast, as we reduced the axon diameter to 9.6 μm, also obtained from the same model, the site of maximum membrane polarization

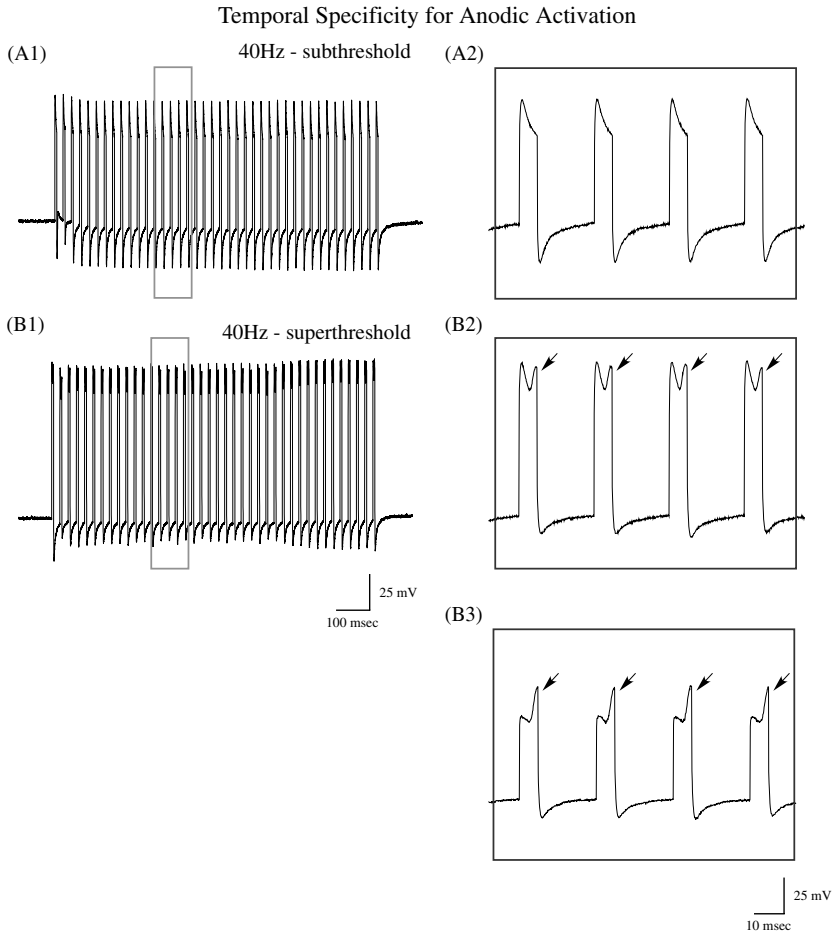

Figure 15. The temporal specificity for anodic activation of an individual neuron demonstrated experimentally ($n = 4$). (A1) A 40 Hz current pulse train of sub-threshold current was applied to an individual neuron (B4/B5) while it was simultaneously recorded intracellularly. No action potentials were induced by this pulse train. (A2) Expanded intracellular recordings corresponding to the boxed area of (A1). (B1) A 40 Hz current pulse train of super-threshold current was applied to the same neuron. Each pulse induced a single action potential on the top of the stimulation artefact, due to the depolarization of the initial axon segments shown in figure 6. (B2) Expanded intracellular recordings corresponding to the boxed area of (B1). (B3) Expanded intracellular recordings corresponding to (B2) when the intracellular recordings of (A2) were subtracted from (B2). In (B2) and (B3), the black arrows point to the peaks of action potentials.

shifted towards the axon hillock (figure 17(B); the grey solid line). These quantitative changes will affect the predicted threshold currents. However, the overall profile of membrane polarization along the neuron did not vary qualitatively with the soma and axon diameters. Therefore, the mechanisms of extracellular ganglionic stimulation will still be valid for various sized neurons when it is applied on the side of the soma opposite to the axon.

What are the effects of dendritic trees on the extracellular stimulation technique? How does the myelination of the axon affect the response to extracellular stimulation applied on the side of the soma opposite to the axon? Since vertebrate neurons have extensive dendritic trees and myelinated axons, this could affect their response. To address these questions, we modified our NEURON model using the geometric parameters of the cat spinal motor neuron from McIntyre and Grill (2000), and replaced the unmyelinated axon with a myelinated axon including nodes of Ranvier and myelinated internodes (figure 18(A); table 3). We measured the membrane polarization along the neuron in this modified model with or without the myelination of the axon as we placed the stimulating electrode both on-axis at $(-221, 0)$ and off-axis at $(-71, 50)$ (figure 18(B); grey dashed and grey solid lines). We then added three dendritic trees surrounding the soma (McIntyre and Grill 2000; table 3). The dendritic trees only had leakage channels in the membrane. We again measured the membrane polarization along the neuron in models that had dendritic trees with or without the myelination of the axon as we placed the stimulating electrode at the identical locations $(-221, 0)$ and $(-71, 50)$ (figure 18(B); black dashed and black solid lines). Lastly, we compared the results under these four conditions. The overall profile of the membrane polarization did not vary qualitatively after adding the dendritic trees on the soma side or after replacing the unmyelinated axon with the myelinated one. However, the site of maximum membrane polarization shifted by one to three axon segments towards the axon hillock. Therefore, the mechanisms of extracellular ganglionic stimulation will still be valid for neurons having various morphologies. As a consequence, this technique could be applicable to vertebrate peripheral ganglia that have cell bodies of neurons clustering near the surface of the ganglia.

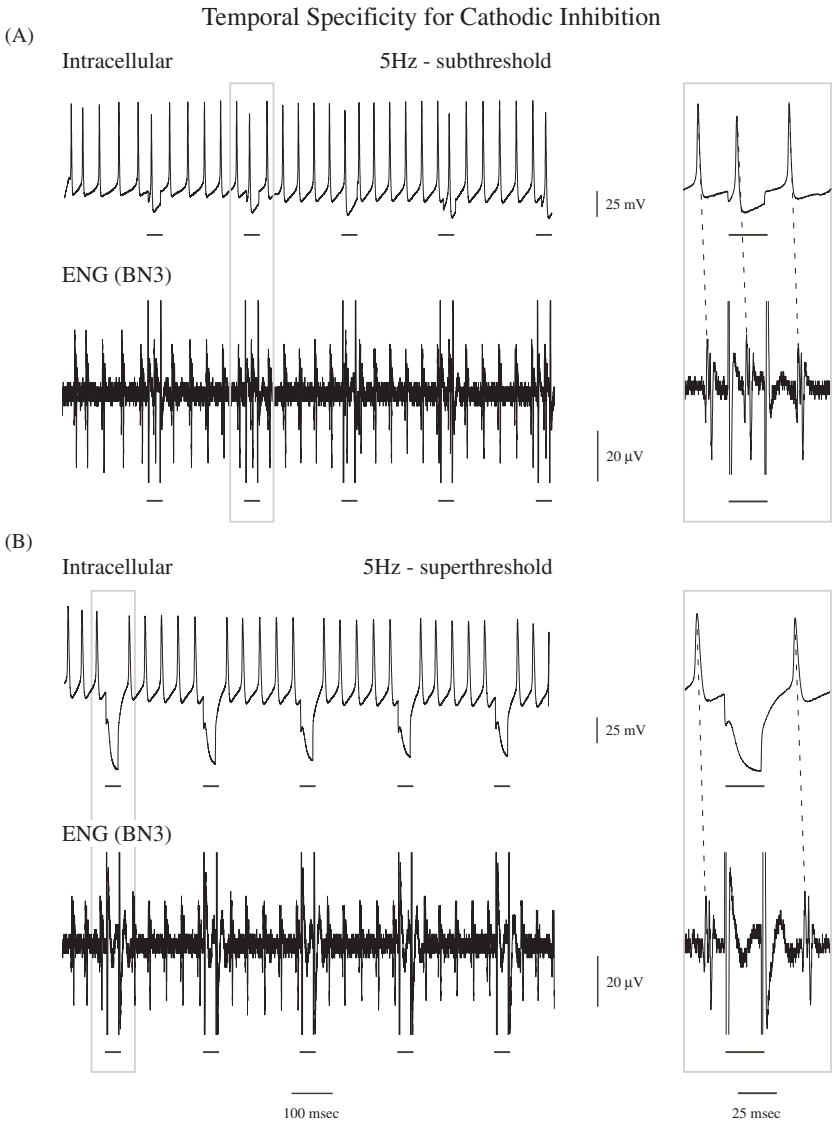

Figure 16. The temporal specificity for cathodic inhibition of an individual neuron demonstrated experimentally ($n = 4$). A 1 s intracellular monophasic pulse was injected into the soma of a neuron (B4/B5) and generated a train of action potentials during this period. The top traces in both (A) and (B) are the intracellular recordings of the neuron. The bottom traces in both (A) and (B) are the extracellular nerve recordings from buccal nerve 3 (BN3) which contains the axon of B4/B5. The boxed areas on the right are the expanded recordings corresponding to the boxed area on the left. Lines underneath traces represent the time of each cathodic extracellular pulse. Dotted lines show corresponding intracellular and extracellular action potentials. (A) A 100 μA 5 Hz cathodic extracellular pulse train was applied above the soma of the targeted neuron during the 1 s intracellular monophasic pulse. Action potentials appeared during the cathodic pulses in both intracellular and nerve recordings. Thus, this sub-threshold cathodic extracellular pulse train did not suppress action potentials. (B) A 250 μA 5 Hz cathodic extracellular pulse train was then applied above the soma of the targeted neuron during the 1 s intracellular monophasic pulse. Action potentials disappeared during the cathodic pulses in both intracellular and nerve recordings. Thus, this super-threshold cathodic extracellular pulse train suppressed action potentials.

Discussion

The objectives of this study were to describe and analyse a technique for selective extracellular stimulation near the cell bodies of ganglia. These results are consistent with earlier modelling studies of the effects of extracellular stimulation on the side of the soma opposite to the axon (Suihko 1998, Rattay 1999). They extend these results in several important ways. To our knowledge, we provide the first intracellular recordings to confirm the change in voltage due to these forms of extracellular stimulation. We also describe the spatial and temporal specificity of the technique in greater detail, and define the windows of specificity, strongly suggesting that the technique could find many practical applications. Six main conclusions can be drawn from this study, which we will discuss in turn.

First, the technique uses anodic currents to activate neurons and cathodic currents to inhibit neurons. The NEURON model predicted that anodic stimulation applied near the soma opposite to the axon activates a neuron by direct depolarization of the initial axon segments (figures 4(A) and 5(A)). Cathodic stimulation applied near the soma opposite

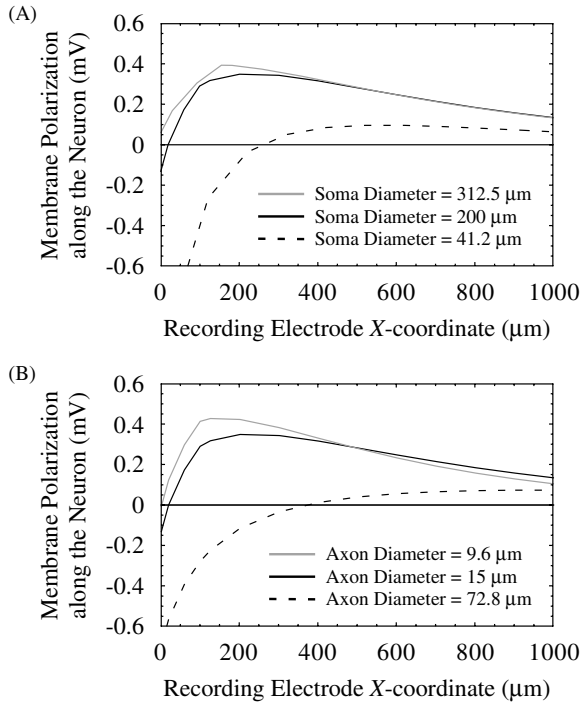

Figure 17. Comparisons of the membrane polarization along a simulated neuron with different soma and axon diameters. (A) The membrane potential changes at the steady state were measured in the NEURON model as we varied the soma diameter alone. A 100 ms anodic current pulse of 10 μA was applied on the axonal axis 50 μm away from the tip of the soma. The black solid line shows the membrane polarization along the neuron with the original soma diameter of 200 μm and axon diameter of 15 μm. The black dashed line shows the membrane polarization along the neuron as we reduced the soma diameter to 41.2 μm, the value for a cat spinal motor neuron (McIntyre and Grill 2000). The grey solid line shows the membrane polarization along the neuron as we increased the soma diameter to 312.5 μm. (B) The membrane potential changes at the steady state were measured in the NEURON model as we varied the axon diameter alone. A 100 ms anodic current pulse of 10 μA was also applied on the axonal axis 50 μm away from the tip of the soma. The black solid line shows the membrane polarization along the neuron with the original axon diameter of 15 μm and soma diameter of 200 μm. The grey solid line shows the membrane polarization along the neuron as we reduced the axon diameter to 9.6 μm, obtained from the same model for a cat spinal motor neuron (McIntyre and Grill 2000). The black dashed line shows the membrane polarization along the neuron with a larger axon diameter of 72.8 μm. Note that the ratios of the soma to the axon diameters are the same for the same style of lines in (A) and (B). Thus, changing the soma and axon diameters in opposite directions will have similar effects on the membrane polarization along the neuron.

to the axon inhibits a neuron by direct hyperpolarization of the initial axon segments (figures 4(B) and 5(B)). In addition, intracellular recordings from two different sites of the soma qualitatively validated the NEURON model's predictions (figures 6 and 7).

Second, the square root of threshold current increases with the distance from the stimulating electrode to the soma (figures 8 and 9), consistent with previous studies by Stoney *et al* (1968) as well as Nowak and Bullier (1996). This allows us to predict the current required to selectively activate or inhibit a neuron at a fixed electrode-to-soma distance. In addition, nerve recordings demonstrated that the sheath of the ganglion does not affect the threshold currents of a neuron during extracellular ganglionic stimulation (figure 10). Thus, this technique can be applied to freely behaving animals.

Third, intracellular recordings from three adjacent neurons demonstrated that an individual neuron can be selectively activated (figure 9) and inhibited (figure 11) by extracellular stimulation near the soma opposite to the axon, which would allow for many scientific and clinical applications. In order to minimize the difficulties of positioning the electrodes precisely over the range of interest, it may be important to develop appropriate multi-electrode devices.

Fourth, our models suggest that this technique could be generalized to any ganglion with cell bodies near its surface. The NEURON model was used to explore the characteristics of spatial specificity of stimulation (figures 12 and 13). The simplified analytical model was used to broadly predict the spatial specificity of arbitrary neurons of various sizes and geometric configurations (figure 14), and provides qualitative insight into the operation of extracellular stimulation that was confirmed by the more quantitative NEURON model.

Fifth, intracellular recordings demonstrated that specific spikes can be added to or removed from the firing pattern of an individual neuron, and thus provide temporal specificity of stimulation (figures 15 and 16). The precise control of spikes will be valuable for clinical applications that minimize side effects, and for scientific experiments.

Finally, modelling studies demonstrate that changing axon or soma diameter, adding dendritic trees or adding myelination do not qualitatively alter the functional actions and mechanism of extracellular stimulation applied on the side of the soma opposite to the axon, although the quantitative effects do change (figures 17 and 18). Interestingly, adding dendrites appears to be similar to increasing soma diameter, moving the initiation or inhibition zone closer to the soma. Qualitatively, this suggests that decreasing the input resistance of the soma or increasing that of the axon will shift the initiation or inhibition zone closer to the soma, as suggested by the analytical model.

Limitations of the NEURON and analytical models

The NEURON and analytical models used in this study had three primary limitations. First, the extracellular saline medium used in both the NEURON and the analytical models was assumed to be homogeneous. In the actual ganglion, there are several sources of inhomogeneity: the sheath, the neuropil including the other embedded cells and the extracellular fluid medium within the ganglion. Some direct experimental evidence supports the hypothesis of homogeneity. In particular, the experimental results showed that the presence of the protective sheath only affected the threshold currents slightly (figure 9). If the assumption of extracellular homogeneity were invalid, the results would be quantitatively different. However, the overall results would still be qualitatively valid.

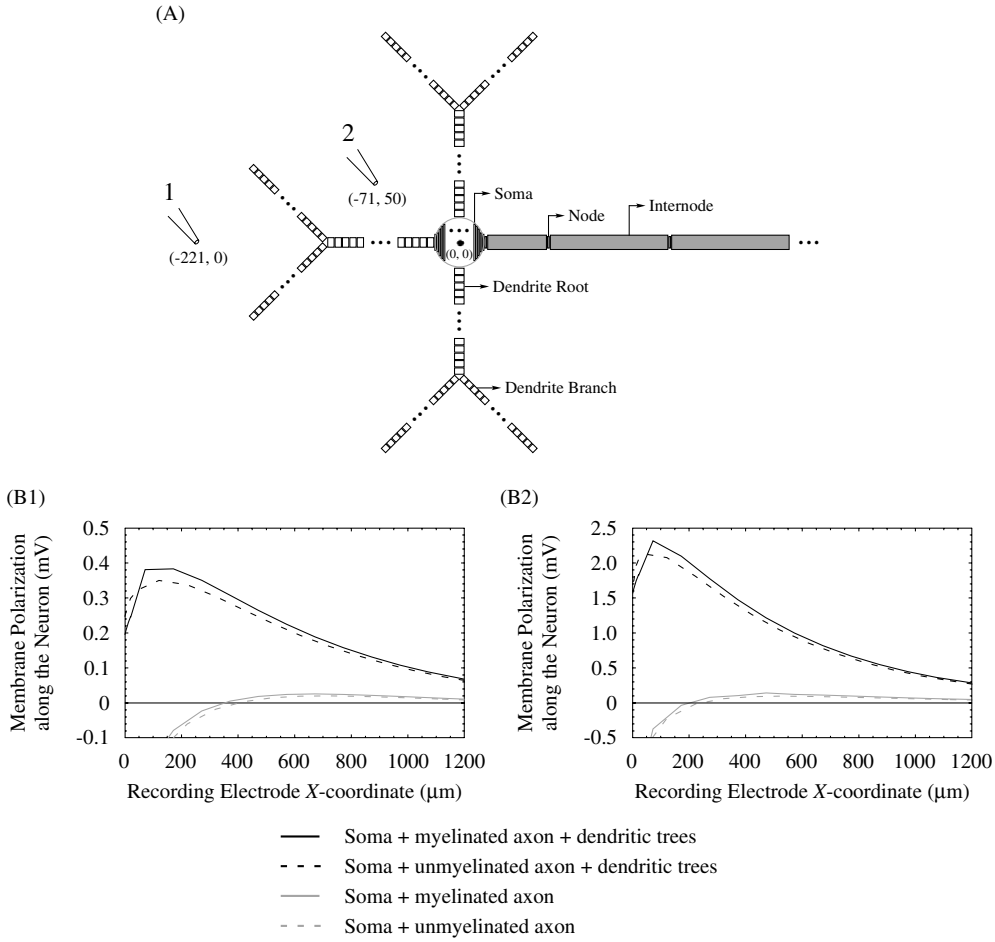

Figure 18. Comparisons of the membrane polarization along the simulated vertebrate neuron with different neuronal structures. (A) Model morphology of the NEURON model of a cat spinal motor neuron using the geometric parameters from McIntyre and Grill (2000). The soma sphere is 41.2 μm in diameter and divided into 100 segments of equal length. The axon is 19 951 μm long and consists of 200 node and internode segments. Each node is 9.6 μm in diameter and 1.5 μm in length, and each internode is 12 μm in diameter and 98.5 μm in length. Three dendritic trees are added to the leftmost, topmost and bottommost tips of the soma. Each of them consists of a dendrite root and two dendrite branches. Each dendrite root or branch is 133 μm in length and divided into 25 equal segments. The diameters are 8 μm and 5.04 μm for the dendrite root and branch, respectively. The centre of the soma is set to be (0, 0). The neuron is stimulated by an extracellular point source electrode at (X_{elec}, Y_{elec}), outside the neuron. (B1) The membrane potential changes at the steady state were measured under four conditions as we applied a 100 ms anodic current pulse of 10 μA on the axonal axis, at (−221, 0). (B2) The membrane potential changes at the steady state were also measured under four conditions as we applied a 100 ms anodic current pulse of 10 μA off the axonal axis, at (−71, 50). In both (B1) and (B2), the grey dashed lines represent the membrane polarization along the neuron consisting of only the soma and unmyelinated axon. The grey solid lines represent the membrane polarization along the neuron consisting of the soma and myelinated axon. The black dashed lines represent the membrane polarization along the neuron consisting of the soma, the unmyelinated axon and three dendritic trees. The black solid lines represent the membrane polarization along the neuron consisting of the soma, the myelinated axon and three dendritic trees. Thus, for both stimulating electrode locations, the overall profile of the membrane polarization did not vary qualitatively after adding the dendritic trees or after replacing the unmyelinated axon with the myelinated one. However, the site of maximum membrane polarization shifted by one to three axon segments towards the soma after adding dendritic trees and myelinating the axon.

Second, both the NEURON and analytical models made several simplifying assumptions that may not apply when the electrode is very close to the soma. For example, both models assumed that the extracellular field was not affected by the neuron, which is not likely to be true at sufficiently short distances (Lee and Grill 2005). In addition, both models did not include the 3D extent of the neuron, which may have different external voltages at different locations surrounding each segment and thus may cause a threshold current error. McIntyre and Grill (1999) showed that the results of the 3D model corresponded closely to the simplified 2D model, with only a 5–10% increase in the relative threshold current value for electrodes positioned over the soma. We have also partially compensated for this potential error by rotating the segments of the soma segments to remain perpendicular to the line connecting the stimulating electrode to the centre of the soma. Furthermore, in the analytical model, we assumed that any line drawn from the stimulating electrode to any point on the axon met the axon at approximately the same angle. This is unlikely to be true at short distances or when the axon curves. Although

all of these effects may be significant at very short electrode-to-neuron distances, they are less relevant at the distances that are likely to be used in experiments.

Finally, the simplified analytical model (equation (4)) is a fit of the full analytical model over a relatively limited range of stimulation distances, from about one to three length constants. Above or below this range, equation (4) starts to deviate significantly from the results of the full analytical model. This limitation can be circumvented by using the full analytical model or by fitting the full analytical model over a different range.

Potential applications of the technique

The ability to selectively stimulate single neurons could allow for many scientific and medical applications. Experimentally, extracellular ganglionic stimulation could be used to study the causal role of an individual neuron on an animal's behaviour. For example, buccal interneurons B4/B5 are strongly activated during rejection in *Aplysia*, whereas they are moderately activated during swallowing and weakly activated during biting (Warman and Chiel 1995, Ye *et al* 2006). By implanting electrodes into freely moving *Aplysia*, one could stimulate B4/B5 selectively, and thus deduce its causal role in the feeding behaviour of *Aplysia in vivo*.

To minimize the difficulties of positioning the electrodes over the surface of ganglia, in current studies in our laboratory, we are developing a multi-electrode device for specific stimulation of individual neurons in any ganglion with cell bodies near its surface. While multi-electrode array devices have been developed for stimulation in the central nervous system, e.g. cortex (McCreery *et al* 2006), spinal cord (Falowski *et al* 2008) and retina (Sekirnjak *et al* 2006), as well as peripheral nerves (Kovacs *et al* 1992), no such device for peripheral ganglia (e.g., autonomic ganglia) has been constructed to date.

Previous work by Tarler and Mortimer (2004) suggested that such a multi-electrode device applied to axons could be used to provide better spatial specificity than a single electrode. Our results suggest that similar specificity could be used to target neuron cell bodies. For example, if a targeted neuron is much smaller than its neighbours with their hillocks aligned, anodic stimulation by a single electrode will lose spatial specificity when the electrode is placed far away from the neurons (figure 14(B)). However, with a multi-electrode device, one could inject anodic currents via the electrode adjacent to the targeted small neuron while injecting cathodic currents via the electrodes adjacent to the neighbouring large neurons, and significantly improve spatial specificity (figure 14(C)). In addition, by combining the spatial and temporal specificity of our technique, such a multi-electrode device could be very useful for selective stimulation of multiple neurons and shaping their firing patterns in different ways, thus generating or switching motor patterns.

Clinically, this technique could be applied to peripheral ganglia to control the activity of the neurons whose cell bodies are near the surface of the ganglion. The pseudounipolar geometry of sensory neurons in these ganglia closely resembles the geometry of the unipolar neurons used in this study (Williams *et al* 1995). In addition, although postsynaptic sympathetic motor neurons have a more extensive dendritic tree, it is likely that it will be possible to selectively stimulate these neurons if their cell bodies are near the surface and their axons are oriented towards the centre of the ganglia (figure 18; Williams *et al* 1995). This may allow greater stimulation specificity than can be achieved by nerve stimulation (Navarro *et al* 2005).

One potential application of the technique described in this paper could be stimulation of the sensory neurons of the vagal ganglia. Vagal nerve stimulation is currently used as a treatment for epilepsy and refractory depression (Shafique and Dalsing 2006). However, its mechanism of action is not well understood, and there are a number of side effects of treatment (e.g., hoarseness, coughing or difficulty breathing). Several of these side effects may be due to the lack of specificity of the stimulation. For example, the current procedure stimulates vagal fibres that branch off to form the recurrent laryngeal nerve. The greater specificity of our technique could allow for equal efficacy with fewer side effects. In addition, it could provide a useful tool for identifying the subpopulation of neurons responsible for the clinical effects of this treatment.

The technique could also be used for many other clinical applications. For example, our extracellular stimulation technique could allow selective inhibition of sensory neurons in dorsal root ganglia for the treatment of chronic pain under conditions such as post-herpetic neuralgia (Holsheimer 1997). Stimulation of postsynaptic neurons in sympathetic ganglia could also be useful under conditions such as urinary incontinence and diabetic autonomic neuropathy (Pedrini and Magnoni 2007).

Acknowledgments

This work was supported by NIH grants NS047073, EB004018 and T32 GM007250, as well as Case Western Reserve University Innovation Incentive Fellowship award. We also thank Dr Cameron McIntyre for helpful discussions at the initiation of the project, and two anonymous reviewers for their comments on an earlier version of the manuscript.

Appendix A

To understand the mechanism of extracellular stimulation over a range of different neural parameters (e.g., conductances, sizes and morphologies), and to predict the threshold current for stimulation without doing extensive, highly realistic simulations (which are computationally expensive), we created an analytical model of extracellular stimulation on the side of the soma opposite to the axon. We represented the neuron as a semi-infinite axon with the tip connected to the extracellular medium through a resistance representing the soma. To simplify the model, we decided to focus primarily on steady-state phenomena; other researches who focus on high frequency stimuli have used an activation function approach to modelling the responses to extracellular stimulation (Rattay

1999). Thus, to model the membrane potential along the axon, we used a steady-state cable equation (Rall and Agmon-Snir 1998) with a position-dependent extracellular field. In essence, this is simply modelling the axon as a wire with a fixed internal resistance per unit length and a fixed membrane conductance to the external medium per unit length. This gives us equation (A.1):

$$\lambda^2 \left(\frac{\mathrm{d}^2 V_{\mathrm{ext}}}{\mathrm{d}x^2} + \frac{\mathrm{d}^2 V_{\mathrm{m}}}{\mathrm{d}x^2} \right) + E_{\mathrm{m}} - V_{\mathrm{m}} = 0, \tag{A.1}$$

where λ is the length constant, V_{ext} is the extracellular field, x is the distance along the axon, V_{m} is the membrane potential and E_{m} is the resting (negative) membrane potential. At this point, it is convenient to rewrite this equation in terms of dimensionless variables both to simplify its form and to clarify the relationships between parameters. Using the extracellular field of a point source (equation (2)) for V_{ext}, equation (A.1) can be non-dimensionalized to yield

$$\frac{2\kappa}{(\alpha + \xi)^3} + \frac{\mathrm{d}^2 \nu}{\mathrm{d}\xi^2} - \nu - 1 = 0, \tag{A.2}$$

where κ is the normalized extracellular current (the extracellular current divided by $-4\pi\sigma_{\mathrm{e}}E_{\mathrm{m}}$, where σ_{e} is the conductivity of the extracellular medium and E_{m} is the resting membrane potential), α is the normalized distance from the centre of the soma to the extracellular stimulating electrode ($\alpha = d/\lambda$, where λ is the length constant of the axon and d is the distance from the centre of the soma to the point current source), ξ is the normalized distance along the axon and ν is the normalized membrane potential ($\nu = -V_{\mathrm{m}}/E_{\mathrm{m}}$). This is a second-order ordinary differential equation, and solving it gives us the following general solution:

$$\begin{aligned} \nu &= c_1 \mathrm{e}^{\xi} + c_2 \mathrm{e}^{-\xi} - 1 + \kappa b_1 \\ b_1 &= \frac{1}{2}\exp(-(\alpha+\xi))\mathrm{Ei}(\alpha+\xi) \\ &\quad - \frac{1}{2}\exp(\alpha+\xi)\mathrm{Ei}(-(\alpha+\xi)) - \frac{1}{\alpha+\xi}, \end{aligned} \tag{A.3}$$

where Ei is the exponential integral ($\mathrm{Ei}(x) = -\int_{-x}^{\infty} (\mathrm{e}^{-t}/t)\mathrm{d}t$) and c_1 and c_2 are constants of integration. To find a particular solution, we assumed that the membrane potential at infinity was the resting membrane potential (i.e. -1 in dimensionless units) and that the potential at the tip of the axon was the sum of the resting potential and the current flowing into the tip of the axon through the soma multiplied by the resistance of the soma:

$$(\nu)_{\xi=0} = 1 - \gamma \left(\left(\frac{\mathrm{d}\nu}{\mathrm{d}\xi} \right)_{\xi=0} - \frac{\kappa}{\alpha^2} \right), \tag{A.4}$$

where γ is the normalized soma resistance ($\gamma = r_{\mathrm{s}}/(r_{\mathrm{i}}\lambda)$, r_{s} is the total resistance across the membrane of the soma and r_{i} is the internal resistance per unit length in the axon). Using these boundary conditions, we found the following general solution for the membrane potential at a position ξ along the axon as a function of the extracellular current κ:

$$\begin{aligned} \nu &= -1 + \kappa(b_1 + b_2) \\ b_1 &= \frac{1}{2}\exp(-\alpha-\xi)\mathrm{Ei}(\alpha+\xi) \\ &\quad - \frac{1}{2}\exp(\alpha+\xi)\mathrm{Ei}(-\alpha-\xi) - \frac{1}{\alpha+\xi} \\ b_2 &= \frac{1}{1+\gamma}\left(\frac{1}{\alpha} - \frac{\gamma-1}{2}\exp(\alpha-\xi)\mathrm{Ei}(-\alpha) \right) \\ &\quad - \frac{1}{2}\exp(-\alpha-\xi)\mathrm{Ei}(\alpha). \end{aligned} \tag{A.5}$$

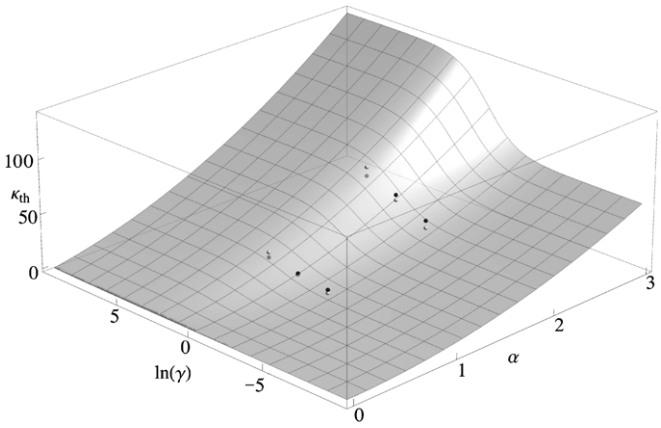

Figure A1. The surface of threshold currents of arbitrary neurons can be predicted as a function of the electrode distance and soma resistance. κ_{th} is the normalized threshold current, $\ln(\gamma)$ is the natural log of the normalized total resistance of the soma and α is the normalized distance to the extracellular current source. See text for further details. The black dots are the normalized threshold currents measured by the NEURON model. The grey dots are the normalized threshold currents predicted by the analytical model.

Note that the membrane potential ν is a linear function of the extracellular current κ. Thus, the point of maximum depolarization or hyperpolarization along the axon is independent of the amount of extracellular current, and the amount of depolarization or hyperpolarization is directly proportional to the current. We can thus, without loss of generality, numerically find the minimum amount of current required to depolarize at least one point on the neuron to the zero potential. This can be done by solving equation (A.5) for κ with ν equal to zero and then adjusting the normalized distance ξ to minimize the value of the normalized current κ, i.e. minimizing the following equation:

$$\kappa = \frac{1}{b_1 + b_2}. \tag{A.6}$$

We call the resulting (minimized) value of κ the normalized threshold current κ_{th} (shown in figure A1). Strikingly, even with pulses of current as short as 6 ms, which were similar to those used for all the anodic stimulation *in vitro*, the results from the NEURON model were quite close to those predicted by the analytical model, suggesting that it may be of use even for moderate frequency stimulation as well as in steady state.

We found that the rational function in equation (4) (with θ set to be 0) provided an excellent approximation to this function, with a maximum error of less than 6% if α is restricted to one to three length constants (or one-fifth to three length constants if γ is greater than 1), which rose to less than 9% with α over a range of two-thirds to four length constants.

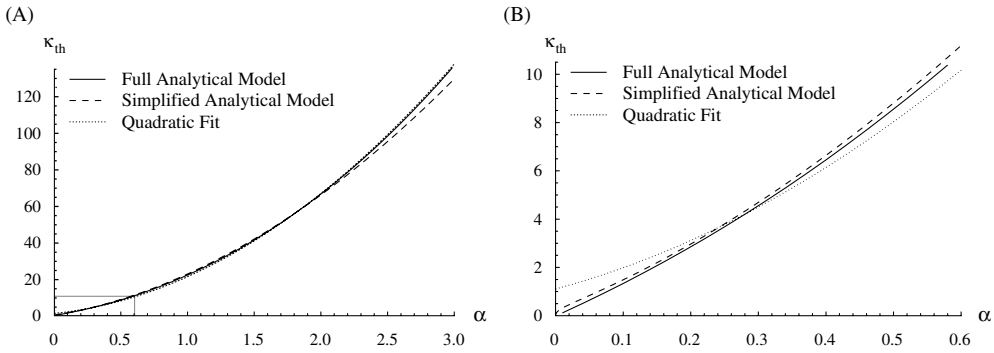

Figure A2. A quadratic fit provides a good approximation for the threshold currents predicted by the analytical model. The solid line shows the predictions of the full analytical model (with $\gamma = 2$), the dashed line shows the prediction of the simplified analytical model (equation (4)) and the dotted line shows a quadratic fit of the full model. (A) While both approximations provide a good fit to the full analytical model, the simplified analytical model is noticeably worse than the quadratic fit at larger distances with this value of γ (which is likely to apply to most values of γ that are experimentally relevant). (B) At shorter distances (corresponding to the boxed region in (A)), the quadratic fit deviates more from the full analytical model than the simplified analytical model.

To provide a simple correction for the angle, the extracellular field can be treated as if it consists of planes of equal potential (as it would be if the source were far away). In this case, an increase in the distance along the axon (e.g., adding an arbitrary constant c to ξ) corresponds to an increase of $c \cdot \cos(\theta)$ in the distance to the source, where θ is the angle between the axon and the line drawn from the current source to the axon (i.e. a vector normal to the isopotential planes). This is equivalent to increasing the conductivity of the medium, σ_e, by a factor of $1/\cos(\theta) = \sec(\theta)$. Since the conductivity of the medium shows up as a divisor of κ, this gives us $\sec(\theta)$ on the right of equation (4). While the choice of the point from which to measure θ is arbitrary at large distances (since the angles are all equivalent), at small distances the angle can vary from point to point. Because the source has the greatest effect on the part of the axon near the soma, it makes sense to choose a point in this area. We found that a point at half of a length constant down the axon provided a reasonable fit to the NEURON model data.

Over most ranges of interest, the behaviour of both the full and the simplified analytical models can be approximated with a quadratic function of α as previously described by Stoney *et al* (1968) and shown in figure A2. This is also suggested by equation (4), with the quadratic term of α clearly dominating as γ becomes very large or very small. This provides a quick heuristic for approximating the threshold function from any three data points. It does not, however, provide an easy way of predicting the fitting parameters before these first data points are collected, nor does it describe the change in membrane potential along the axon. These can be addressed by using equations (4) and (A.5), respectively.

References

Anderson W S and Lenz F A 2006 Surgery insight: deep brain stimulation for movement disorders *Nat. Clin. Pract. Neurol.* **2** 310–20

Barbeau H, McCrea D A, O'Donovan M J, Rossignol S, Grill W M and Lemay M A 1999 Tapping into spinal circuits to restore motor function *Brain Res. Rev.* **30** 27–51

Baxter D A, Canavier C C, Clark J W Jr and Byrne J H 1999 Computational model of serotonergic modulation of sensory neurons in *Aplysia J. Neurophysiol.* **82** 2914–35

Benabid A L, Pollak P, Gao D, Hoffmann D, Limousin P, Gay E, Payen I and Benazzouz A 1996 Chronic electrical stimulation of the *ventralis intermedius* nucleus of the thalamus as a treatment of movement disorders *J. Neurosurg.* **84** 203–14

Cioni B, Meglio M, Perotti V, De Bonis P and Montano N 2007 Neurophysiological aspects of chronic motor cortex stimulation *Neurophysiol. Clin.* **37** 441–7

Cohen M R and Newsome W T 2004 What electrical microstimulation has revealed about the neural basis of cognition *Curr. Opin. Neurobiol.* **14** 169–77

De Ridder D, De Mulder G, Menovsky T, Sunaert S and Kovacs S 2007 Electrical stimulation of auditory and somatosensory cortices for treatment of tinnitus and pain *Prog. Brain Res.* **166** 377–88

Falowski S, Celii A and Sharan A 2008 Spinal cord stimulation: an update *Neurotherapeutics* **5** 86–99

Ferguson G P, Parsons D W, Ter Maat A and Pinsker H M 1986 Spontaneous and elicited bag cell discharges in gonadectomized *Aplysia J. Exp. Biol.* **123** 159–73

Ferguson G P, Ter Maat A, Parsons D W and Pinsker H M 1989 Egg laying in *Aplysia*: I. Behaviour patterns and muscle activity of freely behaving animals after selectively elicited bag cell discharges *J. Comput. Physiol.* **164** 835–47

Gaunt R A and Prochazka A 2006 Control of urinary bladder function with devices: successes and failures *Prog. Brain Res.* **152** 163–94

Hines M L and Carnevale N T 1997 The NEURON simulation environment *Neural Comput.* **9** 1179–209

Hodgkin A L and Huxley A F 1952 A quantitative description of membrane current and its application to conduction and excitation in nerve *J. Physiol.* **117** 500–44

Holsheimer J 1997 Effectiveness of spinal cord stimulation in the management of chronic pain: analysis of technical drawbacks and solutions *Neurosurgery* **40** 990–9

Horridge G A and Bullock T H 1965 *Structure and Function in the Nervous System of Invertebrates* ed T H Bullock and G A Horridge (San Francisco: Freeman) pp 52–3

Hovey M M, Bak A F and Carpenter D O 1972 Low internal conductivity of *Aplysia* neuron somata *Science* **176** 1329–31

Iles J F 2005 Simple models of stimulation of neurones in the brain by electric fields *Prog. Biophys. Mol. Biol.* **87** 17–31

Jezernik S, Craggs M, Grill W M, Creasey G and Rijkhoff N J 2002 Electrical stimulation for the treatment of bladder

dysfunction: current status and future possibilities *Neurol. Res.* **24** 413–30
Kovacs G T, Storment C W and Rosen J M 1992 Regeneration microelectrode array for peripheral nerve recording and stimulation *IEEE Trans. Biomed. Eng.* **39** 893–902
Kreiner T, Kirk M D and Scheller R H 1987 Cellular and synaptic morphology of a feeding motor circuit in *Aplysia californica* *J. Comp. Neurol.* **264** 311–25
Lee D C and Grill W M 2005 Polarization of a spherical cell in a nonuniform extracellular electric field *Ann. Biomed. Eng.* **33** 603–15
Lenarz T, Lim H H, Reuter G, Patrick J F and Lenarz M 2006 The auditory midbrain implant: a new auditory prosthesis for neural deafness—concept and device description *Otol. Neurotol.* **27** 838–43
Levanthal D K, Cohen M and Durand D M 2006 Chronic histological effects of the flat interface nerve electrode *J. Neural Eng.* **3** 102–13
Light T S 1997 *Ewing's Analytical Instrumentation Handbook* 2nd edn ed W E Galen (New York: Dekker) p 1104
McCreery D, Lossinsky A, Pikov V and Liu X 2006 Microelectrode array for chronic deep-brain microstimulation and recording *IEEE Trans. Biomed. Eng.* **53** 726–37
McIntyre C C and Grill W M 1999 Excitation of central nervous system neurons by nonuniform electric fields *Biophys. J.* **76** 878–88
McIntyre C C and Grill W M 2000 Selective microstimulation of central nervous system neurons *Ann. Biomed. Eng.* **28** 219–33
McIntyre C C and Grill W M 2002 Extracellular stimulation of central neurons: influence of stimulus waveform and frequency on neuronal output *J. Neurophysiol.* **88** 1592–604
McNaughton T G and Horch K W 1996 Metallized polymer fibers as leadwires and intrafascicular microelectrodes *J. Neurosci. Methods* **70** 103–10
Mokwa W 2007 An implantable microsystem as a vision prosthesis *Med. Device Technol.* **18** 20, 22–3
Naples G G, Mortimer J T, Scheiner A and Sweeney J D 1988 A spiral nerve cuff electrode for peripheral nerve stimulation *IEEE Trans. Biomed. Eng.* **35** 905–16
Navarro X, Krueger T B, Lago N, Micera S, Stieglitz T and Dario P 2005 A critical review of interfaces with the peripheral nervous system for the control of neuroprostheses and hybrid bionic systems *J. Periph. Nerv. Syst.* **10** 229–58
Nowak L G and Bullier J 1996 Spread of stimulating current in the cortical grey matter of rat visual cortex studied on a new *in vitro* slice preparation *J. Neurosci. Methods* **67** 237–47
Parson D W, Ter Maat A and Pinsker H M 1983 Selective recording and stimulation of individual identified neurons in freely behaving *Aplysia Science* **221** 1203–6
Pedrini L and Magnoni F 2007 Spinal cord stimulation for lower limb ischemic pain treatment *Interact. Cardiovasc. Thorac. Surg.* **6** 495–500
Rall W and Agmon-Snir H 1998 *Methods in Neuronal Modelling—From Ions to Network* 2nd edn ed C Koch and I Segev (Cambridge, MA: MIT Press) pp 27–92
Ranck J B 1975 Which elements are excited in electrical stimulation of mammalian central nervous system: a review *Brain Res.* **98** 417–40
Rattay F 1989 Analysis of models for extracellular fiber stimulation *IEEE Trans. Biomed. Eng.* **36** 676–82
Rattay F 1999 The basic mechanism for the electrical stimulation of the nervous system *Neuroscience* **89** 335–46
Sekirnjak C, Hottowy P, Sher A, Dabrowski W, Litke A M and Chichilnisky E J 2006 Electrical stimulation of mammalian retinal ganglion cells with multielectrode arrays *J. Neurophysiol.* **95** 3311–27
Shafique S and Dalsing M C 2006 Vagus nerve stimulation therapy for treatment of drug-resistant epilepsy and depression *Perspect. Vasc. Surg. Endovasc. Ther.* **18** 323–7
Spelman F A 2006 Cochlear electrode arrays: past, present and future *Audiol. Neurootol.* **11** 77–85
Stoney S D, Thompson W D and Asanuma H 1968 Excitation of pyramidal tract cells by intracortical microstimulation: effective extent of stimulating current *J. Neurophysiol.* **31** 659–69
Suihko V 1998 Modeling direct activation of corticospinal axons using transcranial electrical stimulation *Electroencephalogr. Clin. Neurophysiol./Electromyogr. Motor Cont.* **109** 238–44
Tarler M D and Mortimer J T 2004 Selective and independent activation of four motor fascicles using a four contact nerve-cuff electrode *IEEE Trans. Neural Syst. Rehabil. Eng.* **12** 251–7
Tarver W B, George R E, Maschino S E, Holder L K and Wernicke J F 1992 Clinical experience with a helical bipolar stimulating lead *Pacing Clin. Electrophysiol.* **15** 1545–56
Tehovnik E J, Tolias A S, Sultan F, Slocum W M and Logothetis N K 2006 Direct and indirect activation of cortical neurons by electrical microstimulation *J. Neurophysiol.* **96** 512–21
Tyler D J and Durand D M 2002 Functionally selective peripheral nerve stimulation with a flat interface nerve electrode *IEEE Trans. Neural Syst. Rehabil. Eng.* **10** 294–303
Warman E N and Chiel H J 1995 A new technique for chronic single-unit extracellular recording in freely behaving animals using pipette electrodes *J. Neurosci. Methods* **57** 161–9
Williams P L, Bannister L H, Berry M M, Collins P, Dyson M and Ferguson M W J 1995 *Gray's Anatomy* 38th edn ed M M Berry, S M Standring and L H Bannister (Baltimore: Churchill & Livingstone) pp 945–6, 1259
Winter J O, Cogan S F and Rizzo J F 2007 Retinal prostheses: current challenges and future outlook *J. Biomater. Sci. Polym. Ed.* **18** 1031–55
Ye H, Morton D W and Chiel H J 2006 Neuromechanics of multifunctionality during rejection in *Aplysia californica* *J. Neurosci.* **26** 10743–55
Ziv I, Baxter D A and Byrne J H 1994 Simulator for neural networks and action potentials: description and application *J. Neurophysiol.* **71** 294–308